UPPSALA
UNIVERSITET

Digital Comprehensive Summaries of Uppsala Dissertations from the Faculty of Science and Technology 1410

Single-photon multiple ionisation of atoms and molecules investigated by coincidence spectroscopy

Site-specific effects in acetaldehyde and carbon dioxide

SERGEY ZAGORODSKIKH

ACTA
UNIVERSITATIS
UPSALIENSIS
UPPSALA
2016

ISSN 1651-6214
ISBN 978-91-554-9665-4
urn:nbn:se:uu:diva-301128

Dissertation presented at Uppsala University to be publicly examined in Häggsalen, Ångstömlaboratoriet, Lägerhyddsvägen 1, Uppsala, Friday, 30 September 2016 at 13:15 for the degree of Doctor of Philosophy. The examination will be conducted in English. Faculty examiner: Professor Tom Field (Atomic and Molecular Research Division, School of Mathematics and Physics, Queen's University of Belfast.).

Abstract

Zagorodskikh, S. 2016. Single-photon multiple ionisation of atoms and molecules investigated by coincidence spectroscopy. Site-specific effects in acetaldehyde and carbon dioxide. *Digital Comprehensive Summaries of Uppsala Dissertations from the Faculty of Science and Technology* 1410. 84 pp. Uppsala: Acta Universitatis Upsaliensis. ISBN 978-91-554-9665-4.

In this thesis, multiple ionisation processes of free atoms and molecules upon single photon absorption are studied by means of a versatile multi-electron-ion coincidence spectroscopy method based on a magnetic bottle, primarily in combination with synchrotron radiation. The latter offered the possibility to access not only valence but also core levels, revealing processes, which promote the target systems into different charge states.

One study focuses on double and triple ionisation processes of acetaldehyde (ethanal) in the valence region as well as single and double Auger decay of initial 1s core vacancies. The latter are investigated site-selectively for the two chemically different carbon atoms of acetaldehyde, scrutinising theoretical predictions specifically made for that system.

A related study concentrates on core-valence double ionisation spectra of acetaldehyde, which have been investigated in the light of a previously established empirical model, and which have been used as test cases for analysing this kind of spectra by means of quantum chemical electronic structure methods of increasing sophistication.

A third study investigates site-specific fragmentation upon 1s photoionisation of acetaldehyde using a magnetic bottle augmented with an in-line ion time-of-flight mass spectrometer. Experimental evidence is presented that bond rupture occurs with highest probability in the vicinity of the initial charge localisation and possible mechanisms are discussed. A site-specificity parameter P_Δ is introduced to show that differences in fragmentation behavior between initial ionisations at chemically different carbon atoms probably persist even for identical internal energy contents in the nascent dications.

In another study where both electrons and ions from Auger decay of core-excited and core-ionised states of CO_2 are detected in coincidence, it is confirmed that O_2^+ is formed specifically in Auger decay from the C1s $\rightarrow \pi^*$ and O1s $\rightarrow \pi^*$ resonances, suggesting a decisive role of the π^* orbital in the molecular rearrangement. Also, the molecular rearrangement is found to occur by bending in the resonant states, and O_2^+ is produced by both single and double Auger decay.

A new version of the multi-electron-ion coincidence method, where the ion time-of-flight spectrometer is mounted perpendicularly to the electron flight tube, which affects less the electron resolution and which allows for position sensitive detection of the ions, is employed in combination with tunable soft X-rays to reveal the branching ratios to final Xe^{n+} states with $2 < n < 9$ from pure $4d^{-1}$, $4p^{-1}$, $4s^{-1}$, $3d^{-1}$ and $3p^{-1}$ Xe^+ hole states. The coincident electron spectra give information on the Auger cascade pathways.

Keywords: acetaldehyde, carbon dioxide, xenon, electron correlation, double ionisation, triple ionisation, core-valence ionisation, site-specific Auger decay, multiple Auger decay, branching ratios, site-specific photodissociation, molecular rearrangement, time-of-flight multi-electron-ion coincidence spectroscopy, synchrotron radiation

Sergey Zagorodskikh, Department of Physics and Astronomy, Molecular and Condensed Matter Physics, Box 516, Uppsala University, SE-751 20 Uppsala, Sweden.

© Sergey Zagorodskikh 2016

ISSN 1651-6214
ISBN 978-91-554-9665-4
urn:nbn:se:uu:diva-301128 (http://urn.kb.se/resolve?urn=urn:nbn:se:uu:diva-301128)

List of papers

This thesis is based on the following papers, which are referred to in the text by their Roman numerals.

I **Single-photon double and triple ionization of acetaldehyde (ethanal) studied by multi-electron coincidence spectroscopy**
S. Zagorodskikh, V. Zhaunerchyk, M. Mucke, J. H. D. Eland, R. J. Squibb, L. Karlsson, P. Linusson and R. Feifel
Chemical Physics, **463**, 159–168 (2015).

II **An experimental and theoretical study of core-valence double ionisation of acetaldehyde (ethanal)**
S. Zagorodskikh, M. Vapa, O. Vahtras, V. Zhaunerchyk, M. Mucke, J. H. D. Eland, R. J. Squibb, P. Linusson, K. Jänkälä, H. Ågren and R. Feifel
Physical Chemistry Chemical Physics, **18**, 2535–2547 (2016).

III **Mechanisms of site-specific photochemistry following core-shell ionization of chemically inequivalent carbon atoms in acetaldehyde (ethanal)**
S. Zagorodskikh, J. H. D. Eland, V. Zhaunerchyk, M. Mucke, R. J. Squibb, P. Linusson and R. Feifel
The Journal of Chemical Physics (in review)

IV **Carbon dioxide ion dissociations after inner shell excitation and ionization: The origin of site-specific effects**
J. H. D. Eland, S. Zagorodskikh, R. J. Squibb, M. Mucke, S. L. Sorensen and R. Feifel
The Journal of Chemical Physics **140**, 184305 (2014).

V **Ion charge-resolved branching in decay of inner shell holes in Xe up to 1200 eV**
J. H. D. Eland, C. Slater, S. Zagorodskikh, R. Singh, J. Andersson, A. Hult Roos, A. Lauer, R. J. Squibb and R. Feifel
Journal of Physics B: Atomic, Molecular and Optical Physics **48**, 205001 (2015).

Reprints were made with permission from the publishers.

A list of papers, to which I also have contributed as a part of my Ph.D. studies, but which are not included in this thesis:

- **Complete double valence photoionization study of the electron spectra of krypton**
  P. Linusson, L. Hedin, J. H. D. Eland, R. J. Squibb, M. Mucke, S. Zagorodskikh, L. Karlsson and R. Feifel
  Physical Review A **88**, 022510 (2013).

- **Direct observation of three-electron collective decay in a resonant Auger process**
  J. H. D. Eland, R. J. Squibb, M. Mucke, S. Zagorodskikh, P. Linusson and R. Feifel
  New Journal of Physics **17**, 122001 (2015).

- **Ultrafast Molecular Three-Electron Auger Decay**
  R. Feifel, J. H. D. Eland, R. J. Squibb, M. Mucke, S. Zagorodskikh, P. Linusson, F. Tarantelli, P. Kolorenč and V. Averbukh
  Physical Review Letters **116**, 073001 (2016).

- **Dissociation of multiply charged ICN by Coulomb explosion**
  J. H. D. Eland, R. Singh, J. D. Pickering, C. S. Slater, A. Hult Roos, J. Andersson, S. Zagorodskikh, R. J. Squibb, M. Brouard and R. Feifel
  The Journal of Chemical Physics **145**, 074303 (2016).

- **Relative extent of double and single Auger decay in molecules containing C, N and O atoms**
  A. Hult Roos, J. H. D. Eland, J. Andersson, S. Zagorodskikh, R. Singh, R. J. Squibb and R. Feifel
  Physical Chemistry Chemical Physics (in press)

My contribution to the papers

The results presented in this thesis are based mainly on experimental data obtained during a number of campaigns at the synchrotron radiation facility BESSY II at the Helmholtz Zentrum, Berlin, utilising a state-of-the-art multi-particle correlation method. Effective experimental work in this case requires collaborative efforts of several people in order to solve challenging instrumental issues, which demands qualifications at a high level of understanding of physical processes and the instrumentation.

I have contributed in various ways to all the experimental works presented here, including the planning, preparation and data acquisition, as well as to the scientific discussion of the manuscript drafts in all cases.

In the case of Papers I, II, and III I have taken the main responsibility for the data analysis, including the development of sophisticated data analysis software and the preparation of all the figures as well as writing the initial drafts for these papers with an exception of some parts of Paper II including Figures 5–14 which concern quantum chemical calculations performed by our theoretical collaborators. The drafts were later amended by other co-authors.

I have also played a key role on the software side in particular in the development of a new electron-ion coincidence spectrometer set-up where the electron and ion detection systems are perpendicular to each other presented in Paper V. Furthermore, I have been engaged in mounting and testing of this set-up, especially at BESSY II.

Licence notice

Except where otherwise noted, this work is available under the Creative Commons Attribution-ShareAlike 4.0 International License. To view a copy of this license, visit http://creativecommons.org/licenses/by-sa/4.0/

Any further distribution of this work, its parts or derivatives must maintain attribution to the author and the following link:
http://urn.kb.se/resolve?urn=urn:nbn:se:uu:diva-301128

This notice does not apply to the included papers.

Contents

1. Introduction

The structure of matter on the Ångström (10^{-10} m) scale is governed by electromagnetic interaction and is typically described by quantum theory. At this level matter can be understood in terms of negatively charged electrons and positively charged atomic nuclei, whereby the latter consists of neutrons and protons, being characterised by their mass number A, i.e. the number of neutrons and protons, as well as the atomic number Z, which represents the charge of the nucleus, i.e. the number of protons. Neutral species consist of a balanced number of negative charges (electrons) and positive charges (protons).

According to Bohr's atomic model, electrons surround a nucleus, where they can occupy only a discrete set of stationary orbits. Already Bohr himself was aware of the fact that his model is only of limited use, which led to the development of a more profound theoretical treatment in form of the Schrödinger equation which forms the basis of quantum mechanics. The mathematical solutions of the (non-relativistic) Schrödinger equation for the hydrogen atom, subsequently generalised for systems of $Z+1$ particles, imply energy eigenvalues and *atomic orbitals*. An atomic orbital is typically defined by three quantum numbers: the principal quantum number $n \in [1, +\infty)$, the orbital quantum number $l \in [0, n-1]$ (usually denoted as s, p, d, f, e, ...) and the magnetic quantum number $m \in [-l, l]$. According to the Pauli exclusion principle, each orbital can be occupied by a maximum of two electrons distinguished by different spin quantum numbers $s = \pm 1/2$. These four quantum numbers define spin-orbitals and are commonly used to characterise *quantum states* of the system, which correspond to certain energy eigenvalues. The energy eigenvalue connects to the *ionisation energy,* (binding energy) of an electron, which is the energy required to move an electron into the continuum, i.e. to an infinite distance from the nucleus. Electrons associated with specific orbitals are also often discussed in terms of *shells*, where the principal quantum number denotes main shells, and the orbital quantum characterises sub-shells. Electrons characterised by comparatively high principal quantum numbers (being, on average, further away from the nucleus) are referred to as outer shell electrons or valence electrons, whereas electrons characterised by comparatively low main quantum numbers (being, on average, closer to the nucleus) are referred to as inner shell electrons or core electrons.

Two or more atoms can combine to a molecule by sharing their electrons, which is essential for bond formation. There are different models for describing the formation of molecular orbitals, of which the so-called LCAO (linear combination of atomic orbitals) method is widely used. According to this

method, atomic valence and core orbitals do contribute to the bond formation to a varying degree. Typically, molecular core orbitals retain essentially their atomic character [1] which also leads to the notion of being "localised", whereas molecular valence orbitals can often not be ascribed anymore to a specific atomic contribution, which is the reason why they are usually regarded as being "delocalised". The set and denotation of molecular orbitals depends on the symmetry of the specific molecular system. Moreover, depending on how they contribute to the bond, molecular orbitals can be classified as bonding, anti-bonding or non-bonding.

In order to describe the interaction of light-matter in the quantum world, the concept of photons is used. A photon is an elementary particle, the quantum of all forms of electromagnetic radiation including light. It can be absorbed by an atomic or molecular system and thereby donating its energy to the system. If the amount of energy is sufficient, this can lead to the emission of one or several electrons and, consequently, to the formation of a positive ion, which in the case of molecules may break up into several ionic fragments. These processes are the basic topics of this thesis. The liberation of an electron from a parent atom or a molecule upon photoabsorption is called *photoionisation* and the possible consequent disintegration of molecules is called *photodissociation.*

The technique, that studies the electrons emitted by photoionisation, known as *photoelectron spectroscopy* (PES) has been widely used since the 1960s [2–6]. It measures the electron kinetic energy, which due to energy conservation, is equal to the energy of the absorbed photon minus the ionisation energy of the atomic or molecular orbital of its origin. However, conventional photoelectron spectroscopy techniques have limited possibilities to extract detailed information on *electron correlations*. A simple example represents the case of direct double ionisation initiated by a single photon, forming a doubly charged positive ion without the involvement of a singly ionised intermediate state. Because the two electrons emitted can share the excess energy in an arbitrary manner, a conventional single electron detection method won't be able to reveal how the energy is shared, what final states are formed and what the relative intensity ratio of the possible different final states are.

In contrast, TOF-PEPECO, the time-of-flight photoelectron-photoelectron coincidence spectroscopy, technique originally devised by John H. D. Eland and coworkers at Oxford [7], offers much more versatile electron spectroscopy studies, allowing to detect in coincidence all the electrons originating from the same ionisation event and thus to obtain knowledge about their energy correlations. It was utilised in this thesis in Papers I and II to study multi-ionisation processes in acetaldehyde. A further development of this technique named time-of-flight photoelectron-photoelectron-photoion-photoion coincidence (TOF-PEPEPIPICO) spectroscopy [8] involves coincidence detection of both multiple electrons and ions related to the same ionisation event. It enables a more thorough description of the fates of photoionised atoms and molecules, including information about the fragmentation patterns resulting

from different possible photoionisation routes. It also provides direct information on the final charge states of the products, which allows the investigation of, for instance, branching ratios. The TOF-PEPEPIPICO technique has been employed in Papers III, IV and V. Alternative, powerful coincidence spectroscopic techniques, which are sensitive to electrons and/or ions, are e.g. threshold photoelectron coincidence (TPESCO) [9] and cold target recoil ion momentum spectroscopy (COLTRIMS) [10]. Furthermore, the technique of velocity map imaging (VMI) [11], which can be used for the studies of electrons and ions, is more and more commonly used for coincidence experiments. In Paper V a new TOF-PEPEPIPICO set-up with perpendicular mounting of the mass spectrometer in respect to the electron detector has been introduced, parts of which are also suitable for VMI detection, although this compatibility has not been fully exploited in the work presented.

One of the samples studied in this work is acetaldehyde or, according to the systematic chemical nomenclature, ethanal. Its structural formula is shown in Figure 1.1. The molecule can be considered to consists of two groups: formylic ($-$CHO) and methylic ($-CH_3$). The hydrogen atoms have only one electron each contributing to the bonds, while the oxygen and carbon atoms, which are elements of the second row of Mendeleev periodic table, give strong contributions to the bonds primarily with their $n = 2$ electrons. The remaining O1s, formylic C1s and methylic C1s orbitals do also contribute to the bonds, but at a much lesser degree and are considered to be essentially atomic-like. Due to the different chemical environment the two carbon 1s orbitals have a difference in ionisation energy of a few eVs. This opens up the possibility to study photoionisation properties of acetaldehyde *site-specifically* (or site-selectively), i.e. depending on the involvement of one or the other C1s orbital. Paper I studies site-specific single and double Auger decay, while Paper III investigates site-selective photodissociation upon $C1s^{-1}$ and $O1s^{-1}$ core ionisation. Paper II concentrates on core-valence double ionisation spectra of acetaldehyde, which could not be studied site-specifically for the two different carbon sites for reasons explained later, but which are found to represent essentially a superposition of two core-valence processes involving the two C1s orbitals.

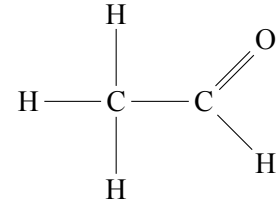

Figure 1.1. Structure of acetaldehyde.

Paper IV studies dissociation of carbon dioxide upon normal or resonant Auger decay and examines some hypothesis from previous works, such as the mechanisms for the formation of O_2^+ ions, which cannot originate from pure bond breakage in the case of carbon dioxide. Finally, Paper V investigates the ion charge state branching in Xenon for pure inner shell hole states, going beyond previous studies of this system.

2. Photoionisation

2.1 Photoelectric effect

The phenomenon of electron emission by matter exposed to electromagnetic radiation is called the *photoelectric effect* and was discovered by Heinrich Hertz in 1887 [12]. It is typically observed by using two metal electrodes in vacuum. One of them is exposed to the radiation, which leads to emission of electrons. This results in electric current between the electrodes, measurable with an ammeter. However, if the frequency of the radiation was below a certain threshold no photocurrent was observed, regardless of the radiation intensity available at the time. This threshold was found to be characteristic for different materials. The existence of thresholds contradicts classical electrodynamics, which predicts that the radiation of lower frequency transfers its energy to almost free electrons in metals more efficiently.

The theoretical explanation given by Albert Einstein [13] in 1905 was based on the quantisation of electromagnetic radiation, with the energy of the quanta directly proportional to the frequency. If the radiation can be absorbed only as individual quanta, then for any frequency below the threshold there is simply not enough energy to extract an electron. This is the basis of *Einstein's photoelectric law*, which can be denoted as

$$E = h\nu - W \tag{2.1}$$

where E is kinetic energy of the emitted electron and W is the work function, i.e. the minimum energy required to remove an electron. It is defined by the properties of the electrode material. Planck's constant, h, relates the frequency, ν, and the energy of the quantum of radiation called the *photon*. This model laid the foundation for the subsequent development of quantum theory and to the modern conceptions of atomic and molecular structure. As credit for the discovery of the photoelectric law, Einstein was awarded the 1921 Nobel Prize in Physics.

Equation (2.1) plays a central role in the photoionisation. For free atoms and molecules W in Equation (2.1) is commonly referred to as *ionisation energy* (or binding energy) and is understood as the energy required to remove an electron from a particular orbital. Electrons in different shells and subshells of the same atom or molecule in most cases have different ionisation energies, therefore, in measuring their ionisation energies one can characterise the elec-

tronic structure of the sample. In the simplest case, when a single photon gets absorbed by one electron, the ionisation energy can be denoted as

$$I = h\nu - E. \tag{2.2}$$

It should also be noted, that after the invention of lasers [14–16] in the late 1950s, it became possible to involve much higher radiation intensities in experiments on the photoelectric effect, which led to the revelation of multiphoton absorption [17]. In such cases, the concept of a threshold in the photoelectric effect is still holds, but instead of a single photon several photons of lower energies deliver together sufficient energy to overcome this threshold. Consequently, Einstein's law is still valid for such processes, but $h\nu$ needs formally to be exchanged by $Nh\nu$, where N is the number of the absorbed photons.

In this work only single photon processes are studied. But such photon does not necessarily transfer its energy to only one electron. In such cases a single photon multiple photoionisation occurs.

2.2 Auger effect

The Auger effect was discovered in the 1920s almost simultaneously by Lise Meitner [18] and Pierre Auger [19]. In the simplest case, when there are three electrons involved it is typically described as a two-step process, while an Auger process involving more steps is called *Auger cascade.* The photon energy needs to be above the ionisation energy of an inner shell electron, extracting it to the continuum in the first step as shown in the left panel of Figure 2.1(a). The positively charged product then has a vacancy, called a *core hole*, which tends to decay within a few femtoseconds.

The core hole state can, in general, decay in two ways. In both cases some electron from the outer shell fills the core hole releasing the excitation energy of the ion. The energy can be either emitted as a photon or it can be transferred to a third electron, called the *Auger electron,* which escapes the system as shown in the right panel of Figure 2.1(a). Heavier elements tend to decay more radiatively, while the elements of the second row of the Mendeleev periodic table, such as carbon and oxygen, decay predominantly within the framework of the Auger effect [20].

The final state of the described process is dicationic with two vacancies in the valence shell. Its energy relative to the ground state of the parent atom or molecule is called *double ionisation energy* and can also be understood as the energy required to remove two electrons corresponding to the vacancies from the initial neutral molecule. It can be represented as

$$I = I_d + I'_a = I_c - E_a \tag{2.3}$$

where I is double ionisation energy, I_d is the ionisation energy associated with the orbital where the deexcited electron originates from, I'_a is the ionisation

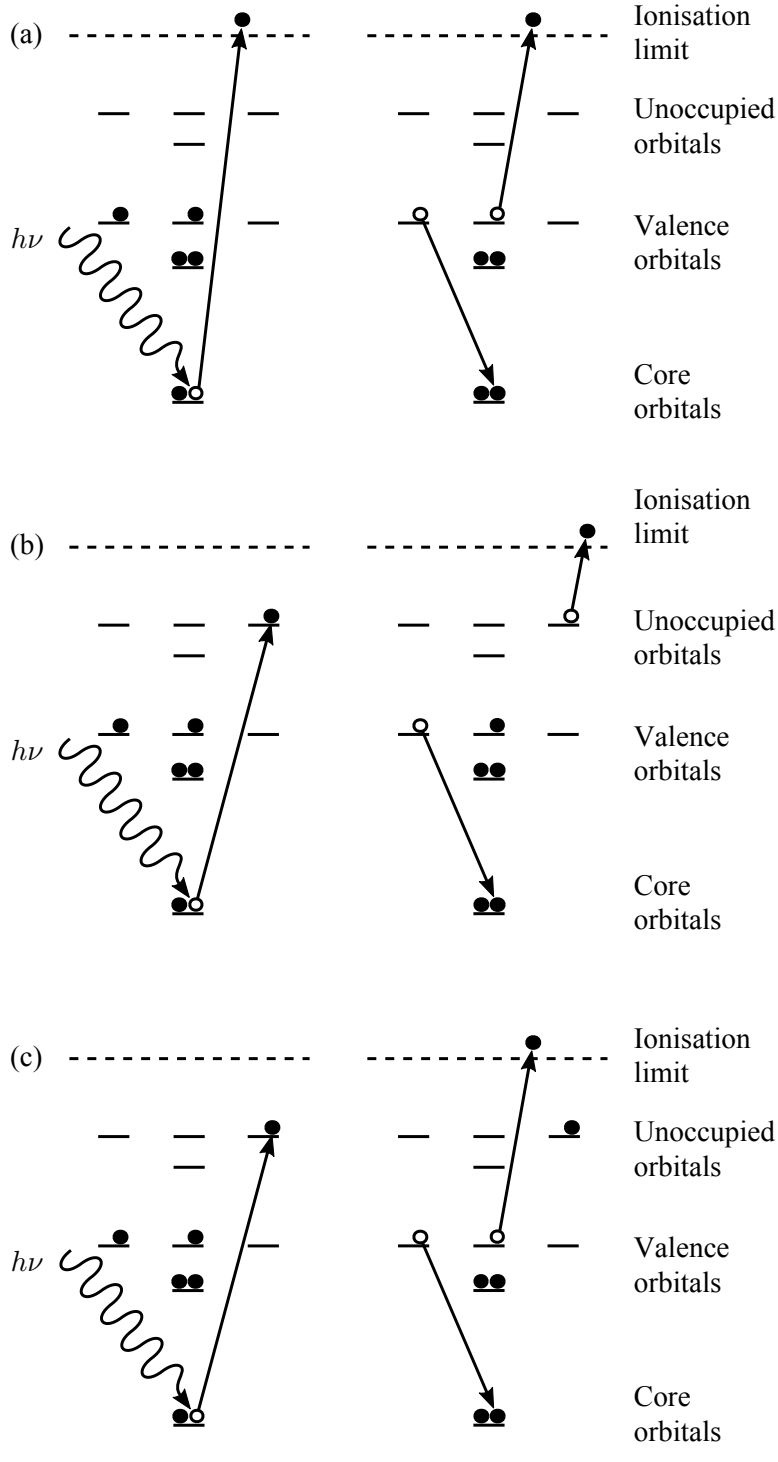

Figure 2.1. Illustration of (a) normal, (b) resonant participator and (c) resonant spectator Auger decay.

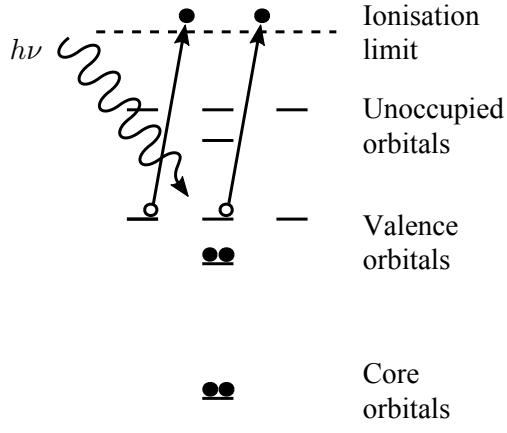

Figure 2.2. Illustration of direct double valence ionisation.

energy of the Auger electron, I_c is the ionisation energy of the core electron and E_a is the kinetic energy of Auger electron. The apostrophe denotes the change in the ionisation energies in the ion as compared to the initial neutral atom or molecule due to the orbital relaxation when the number of electrons in the system decreases in the core ionisation. However, in comparison to alternative pathways, such as valence double ionisation, discussed in the next chapter, leading to the same final dicationic state, this change does not affect the value of the double ionisation energy.

The Auger process described above is typically called *normal* in contrast to *resonant* Auger decay, which implies an inner shell excitation instead of ionisation in the initial step. Consequently, in the simplest case the final state is singly ionised. The name "resonant" is attributed to the fact that it requires the photon energy to match the energy difference between the orbitals involved in the excitation process. The process can be either of *participator* or *spectator* type as illustrated in Figures 2.1(b) and 2.1(c), respectively. In the former case, the previously excited electron is involved in the decay, while in the latter case it does not take part in the process.

Furthermore, in case if in Auger decay the vacancy is filled by an electron from higher subshell of the same shell, the process is called *Coster-Kronig transition.*

2.3 Direct multiple photoionisation

Direct multiple photoionisation is the phenomenon where two or more electrons ejected from the atom or molecule by one photon in a single step, i.e. without involvement of any intermediate state in the ionic product.

Figure 2.2 illustrates direct double valence photoionisation by a single photon. In building on Einstein's photoelectric law, the double ionisation energy can be expressed as

$$I = h\nu - E_1 - E_2 \tag{2.4}$$

where E_1 and E_2 are the kinetic energies of the two emitted electrons. This can be easily generalised to the case of direct ionisation of higher orders:

$$I = h\nu - \sum E_i \tag{2.5}$$

where i is the index of an ionised electron.

The sum of the kinetic energies of all electrons extracted in one step, which is equal to $h\nu - I$ is referred to as the *excess energy*. It has a specific value for a given photon energy and final state. However, its distribution between the electrons is not uniquely defined, i.e. the excess energy can be shared between the electrons with different proportions having different probabilities. In the case of two electrons involved, where the excess energy is below about 10 eV, it is almost equally likely to detect electrons close in kinetic energy and pairs where one of them received much higher energy portion than its counterpart, i.e. the distribution is essentially flat. Higher excess energy results in increasingly unequal distribution and less pairs close in energy, than those with more significant difference. In the literature [21–23] typically three mechanisms are distinguished:

- *Knock-out,* or two-step-one, which implies that the the energy of the photon is transferred to one electron, which before leaving the parent atom or molecule collides with another electron donating to it some part of the excess energy. The model was proposed in 1990 by James Samson based on the similarities between double photoionisation with the ionisation by electron impact [24].
- *Shake-off,* which is based on similarities with secondary ionisation following β^--decay of the nucleus [23, 25]. It assumes, that the first electron escapes the system so fast, that the potential of the system changes very quickly in comparison to the period of motion of the bound electrons (sudden approximation). In this case, the bound electrons feel the new configuration of the electromagnetic field before they relax, which implies some probability that one or several electrons can be "shaken-up" to an unoccupied orbital or "shaken-off" to the continuum.
- *Quasifree,* which was proposed by Amusia *et al.* [26] in 1975 and only recently proven to exist [27]. Its fingerprint is the ejection of two electrons back to back with equal energy sharing, while the nucleus stays in rest. However, as also mentioned in Ref. [27], its contribution to the total amount of double photoionisation is less than 1% at least in the case of Helium.

2.4 Photodissociation

In molecules the valence orbitals strongly contribute to chemical bond formation. The removal of one or more electrons, in particular, from bonding molecular orbitals, may result in the molecule breaking apart. Fragmentation patterns generally depend on the electronic states and in some cases, on the ionisation path. In the case of multiple ionisation, the resulting multiple positive charges in the ionic products repel each other electrostatically, which leads to dissociation, possibly with high kinetic energy of the products, which is referred to as *Coulomb explosion.*

One interesting case of photodissociation is *molecular rearrangement*, that is the appearance of fragments, which are not expected to originate from only rupture of bonds in the target molecule. It means, that upon breaking bonds, sometimes it is possible, that new bonds are formed. Paper IV presents the study of this phenomenon in the case of photoinduced dissociation of carbon dioxide, which leads to the formation of O_2^+ product.

Another series of investigations concern the putative possibility to control the dissociation of large organic molecules by creating core holes, either by ionisation or excitation, localised on particular molecular sites. The prospective idea is sometimes called *molecular scissors*, which would enables a possibility to "cut" such molecules precisely at the desired bond and could be instrumental in chemical and biological applications [28]. As carbon is the basis for organic molecules, it is a species of good interest in this respect. Paper III is devoted to photodissociation of acetaldehyde, where the bond rupture was investigated site-specifically for initial ionisation of either methylic or formylic C1s core level, which can be considered as a step towards the prospective development of molecular scissors.

3. Experimental

3.1 Photoelectron spectroscopy

Photoelectron spectroscopy (PES) was developed from the 1960s on by several research groups. The most prominent were: David W. Turner's group [2] at Imperial College London and later on at Oxford University, the group lead by Fyodor Ivanovich Vilesov [3, 4] at Leningrad State University and by Kai Siegbahn and his group [5, 6] at Uppsala University, who coined the name "Electron Spectroscopy for Chemical Analysis" (ESCA). In 1981 Siegbahn was awarded the Nobel price in Physics in honour for his contribution to the development of this technique.

The idea of photoelectron spectroscopy is to study the electronic properties of matter exposed to ionising electromagnetic radiation by measuring the kinetic energies of the emitted electrons. It can reveal information on the energy levels of a particular substance and mechanisms of the photoionisation processes, determine the chemical composition of a sample and distinguish bulk and surface electronic properties in solids, which leads to many applications of this technique.

Depending on the energy of the radiation source, photoelectron spectroscopy is usually divided into ultraviolet photoelectron spectroscopy (UPS) and X-ray photoelectron spectroscopy (XPS). UPS employs photon energies in the range of tens of eVs, which corresponds to the vacuum ultraviolet (VUV) radiation, and concentrates mainly on the ionisation processes involving valence shells. Since valence electrons are delocalised, UPS allow study of the macroscopic properties of solids, such as band structure, as well as the molecular orbital structure and bond formation in the case of molecules.

X-ray photoelectron spectroscopy is associated with the photon energy range of hundreds of eVs, up to several keVs, which corresponds to the X-ray region of the electromagnetic spectrum. Photons of such energies are able to ionise not only valence, but also core shell electrons or promote them to unoccupied orbitals. Since core electrons

Table 3.1. *1s electron ionisation energies of the first and second row elements of the Mendeleev periodic table in their pure forms. Values are taken from [29] with additional corrections made in [30].*

Z	Symbol	I (eV)
1	H	13.6
2	He	24.6
3	Li	54.7
4	Be	111.5
5	B	188.0
6	C	284.2
7	N	409.9
8	O	543.1
9	F	696.7
10	Ne	870.2

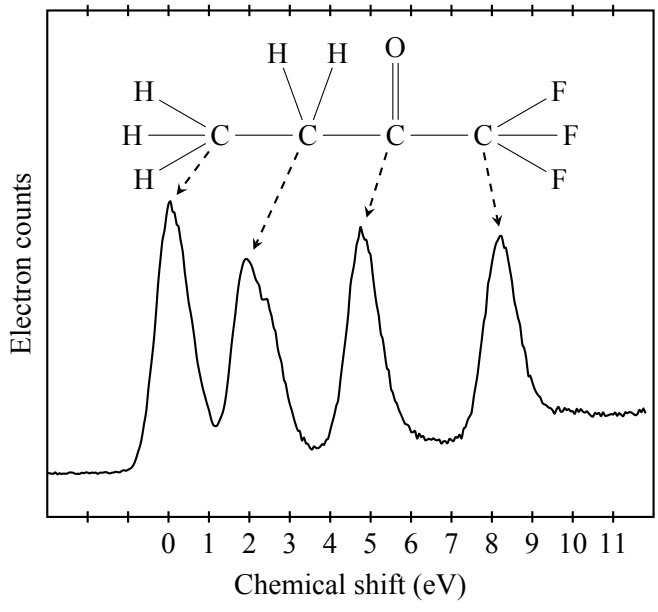

Figure 3.1. X-ray photoelectron spectrum of carbon 1s ionised ethyl trifluoroacetate, which consist of four carbon atoms in different chemical environments. The data displayed were measured by our research group [31].

are localised, which implies that in molecules core orbitals are essentially atomic-like, X-ray photoelectron spectroscopy has a local selectivity. This implies that in the case of free molecules that one can study the properties of different sites in a molecular system. Another aspect of XPS is element-sensitivity. Core ionisation energies can be regarded as fingerprints of chemical elements, which is the basis of the historical name "Electron spectroscopy for chemical analysis". Examples are given in Table 3.1, where the ionisation energies of 1s electrons are listed for the elements of the first and second row of the Mendeleev periodic table. Using such well-known energies one can utilise the technique in odrer to reveal the composition of samples in the gas and condensed phase [6].

In molecules and condensed matter, core levels are affected by the surrounding atoms. This effect can be regarded being small compared with the differences between ionisation energies of different elements, but it can be revealed as shifts of the core photoelectron lines by a few eVs. This phenomenon is called *chemical shift* and is particularly useful to investigate the chemistry of surfaces. Applied to free molecules it enables the possibility to study a particular site of a molecule with several atoms of the same element in different chemical environments, such as the example spectrum in Figure 3.1. It represents the data for ethyl trifluoroacetate, which is the molecule for which the phenomenon was originally observed by Kai Siegbahn. The chemical shift

is typically derived as the ionisation energy above threshold, i.e. above the energy of the lowest core ionised state for the atoms of given element in the particular molecule.

Another kind of electron spectroscopy is Auger electron spectroscopy (AES). It studies the electrons emitted upon the removal or excitation of a core electron, which was described before in §2.2. In the case of the normal Auger process, it gives information on the energies of doubly ionised (dicationic) final states. Every such state is defined by its configuration, that is a pair of vacancies in the valence shell. According to Equation (2.3) in normal Auger decay, unlike for the photoelectron lines, the energy of an Auger electron does not depend on the energy of the absorbed photon. In changing the photon energy, the Auger peaks may change only intensities and profile, but not their positions. They disappear when the photon energy goes below the corresponding core ionisation threshold. Since the photoelectrons always shift in their kinetic energies with modification of the photon energy, this provides an easy way to experimentally distinguish between Auger and photoelectron lines. Also, it implies that non-monochromatic sources, such as X-ray tubes can be used for Auger electron spectroscopy in many cases. A common application of using this technique is surface analysis. In the present work the Auger spectra of free atoms and molecules were measured.

3.2 Magnetic bottle time-of-flight correlation spectrometer

3.2.1 Coincidence measurements

The experimental technique utilised in this work concerns studies of multiple electron emission processes upon single photon absorption. This provides a possibility to investigate processes such as direct multiple photoionisation (§2.3) as well as to study both normal and resonant Auger decays (§2.2) and photodissociation (§2.4) in an element-specific and site-specific manner.

In the ideal case we want to detect all electrons originating from each single photon absorption event and to be able to associate different electrons from one such event to each other. In order to approach this goal, the experimental set-up needs to fulfil several requirements:

- A detector with multi-hit capability, in order to handle several almost simultaneously emitted electrons.
- High electron collection efficiency, which includes the ability of the spectrometer to direct the electron to the detector and detector's capability to register an electron. Otherwise the acquisition time needs to be substantially extended, which may become impractical, in particular taking into account, that most of the work is done at a synchrotron radiation facility with very limited amount of time available.

- High acceptance angle. Although directly related to the collection efficiency, it has an importance in its own, since even if one detects all the electrons emitted in only half of the solid angle, the other half would be lost. It would not make it possible to correlate electrons emitted back-to-back as for instance in the case of quasifree mechanisms of double ionisation described in §2.3.
- Capability to detect electrons within a relatively wide range of kinetic energies simultaneously with reasonably high resolving power. In the case of classical non-coincidence experiments employing a conventional electrostatic hemispherical analyser one can tune the voltages in order to select a very narrow range of kinetic energies of interest. However, in coincidence experiments one is very often interested in correlations between electrons with substantially (up to few hundreds eVs) different in kinetic energy. Therefore it is very important that the high collection efficiency is nearly constant over a larger range, than in the case of non-coincidence studies.
- Coincidence conditions, i.e. the possibility to almost certainly attribute detected particles to the same ionisation event involving a specific atom or molecule.

All these goals are achieved in the presented work using a spectrometer based on the combination of strong and weak magnetic fields described in the rest of this section.

3.2.2 Magnetic bottle principle

The magnetostatic Lorentz force, $\vec{F}$ applied to an electron is

$$\vec{F} = -e[\vec{v} \times \vec{B}] \tag{3.1}$$

where e is the elementary charge, $\vec{v}$ is the velocity vector, $\vec{B}$ is the magnetic induction vector and the symbol $\times$ denotes the cross product. As it can be seen from Equation (3.1) the force is always perpendicular to the velocity vector, which means, that it can change the direction, but not its magnitude and therefore does not change the kinetic energy of the electron.

In the case of a uniform magnetic field, the velocity component, parallel to the magnetic field $v_{\parallel} = v\cos\theta$, is not affected by this field (θ is the angle between the vectors $\vec{v}$ and $\vec{B}$). If the component $\vec{v}_{\perp}$ (two-dimensional vector) is non-zero, the projection of the electron onto the plane perpendicular to $\vec{B}$ performs circular and uniform motion. The centripetal acceleration, a, of such motion is

$$a = \frac{v^2}{r} \tag{3.2}$$

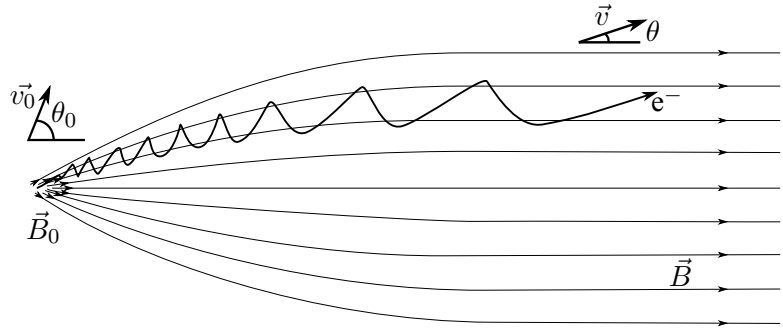

Figure 3.2. On the magnetic bottle principle explanation.

where r is the radius of the trajectory. From Equation (3.1) we can obtain

$$a = \frac{e}{m} v_\perp B \tag{3.3}$$

where m is the electron mass. Combining the last two equations, we get the expression for the radius

$$r = \frac{m v_\perp}{eB}. \tag{3.4}$$

Let us consider a non-uniform magnetic field, that has a small monotonic gradient in the direction of $\vec{B}$. Here "small" means that the magnitude of the field changes negligibly within one cycle of the electron helical motion. Such a field configuration is shown in Figure 3.2 and called *magnetic bottle* or *magnetic mirror*.A spectrometer utilising this field configuration was first presented by Kruit and Read [32] in 1983. In this figure θ_0 and $\vec{v_0}$ denote the initial angle and velocity of the emitted electron, while B_0 the magnitude of the magnetic field in the initial position of the electron. The angular momentum $L = rmv_\perp$ is a conserved quantity in this case [33, 34]. Since the mass is constant, we can write:

$$r_0 v_{0\perp} = r v_\perp \tag{3.5}$$

Here r_0 is the initial radius of the circular projection of the motion. Using Equation (3.4) we can find the expression for $v_\perp$:

$$\frac{m v_{0\perp}}{eB_0} = \frac{m v_\perp}{eB}, \tag{3.6}$$

which is transformed to

$$v_\perp = v_{0\perp} \sqrt{\frac{B}{B_0}}. \tag{3.7}$$

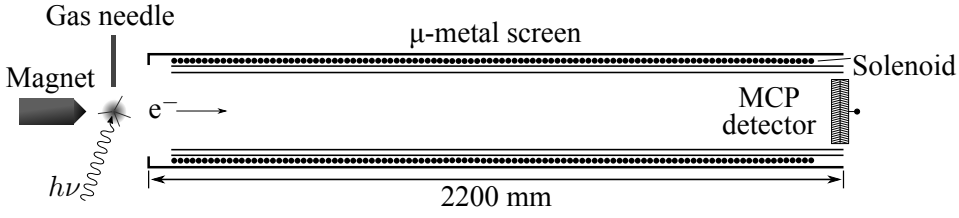

Figure 3.3. Illustration of the magnetic bottle time-of-flight correlation spectrometer.

Accordingly, the velocity component perpendicular to $\vec{B}$ increases while the particle is travelling from the weaker to the stronger magnetic field region and vice versa. Since the magnitude of the total velocity is not changed by the magnetic field, the parallel component $v_{\parallel}$ changes in opposite way to B. This results in the effective mirroring of the particle. In the case of the electron being emitted with the $\theta_0 > \pi/2$, i.e. initially moving towards the stronger magnetic field region, its velocity will eventually become completely perpendicular to $\vec{B}$. At this point a fluctuation of $v_{\parallel}$ towards the stronger magnetic field region will be extinct, while a deviation towards the weaker field will be amplified and the electron will be directed towards the volume with smaller B.

Solving the system of Equations (3.4) and (3.5) relative to the ratio of radii, one can get:

$$\frac{r}{r_0} = \sqrt{\frac{B_0}{B}} \tag{3.8}$$

which leads to another, more comprehensible explanation. The magnetic flux (i.e. the number of field lines) through the circular projection of the trajectory in the plane perpendicular to $\vec{B}$ is constant. Since the lines diverge toward the weaker field region, the radius of the circle increases with smaller B, and since the magnitude of v does not change, higher r means faster motion parallel to B, i.e. all the electrons, regardless of their initial velocity direction are guided towards the weak field region.

3.2.3 Set-up for electron only detection

The above principle is the basis of the electron spectrometer, which has been used in all the experiments in the present work. It first was realised to be powerful for coincidence studies by John H. D. Eland *et al.* [7] in 2003 and has since then extensively been used by our research group as well as other groups [35, 36].

A schematic illustration of the spectrometer is shown in Figure 3.3. A strong (about 1 T at the tip) conical permanent magnet and a relatively weak (few mT) magnetic field of the solenoid constitute the magnetic bottle in this case. Perpendicular to the field lines, which are arranged to confine at the radiation-

matter *interaction region*, there is an effusive needle used to introduce the gaseous sample. The backing pressure, i.e. the pressure in the chamber when there is no flow of sample, is usually on the order of 10^{-7} mbar, while the pressure in the presence of a sample is normally one order of magnitude higher. This provides a good signal to background ratio and at the same time reduces the probability for collisions between the ionisation products and surrounding background molecules.

Highly monochromatic VUV or X-ray radiation pulses are delivered to the interaction region perpendicularly to both the gas needle and the magnetic field lines. More than 95% of the electrons emitted into the whole solid angle of 4π are directed into an about 2.2 m long flight tube surrounded by a homogeneous magnetic field, created by the solenoid, as well as by a μ-metal shield. The tube is terminated at the other end by a *Micro-channel plate* (MCP) detector. The detector is the main limiting factor for the collection efficiency, since, because of the porous structure of the microchannel plates, it is able to detect only about half of the electrons. Using the time reference from the radiation source, we measure the flight time of the electrons through the tube and convert it to kinetic energy. The resolving power of the instrument used for this thesis work is nearly constant and about $E/\Delta E \approx 50$. That is the slower the electron, the better is the resolution.

In order to achieve coincidence conditions, the intensity of the radiation is adjusted to provide a comparatively low probability of ionisation of each sample atom or molecule in the interaction region resulting in ionisation events occurring on average only one in several tens or hundreds of the radiation pulses. In this case the probability of two or more sample species to be ionised by the same pulse is negligible. Coincident events comprising electrons, originating not from the same atom or molecule are referred to as *accidental*.

In comparison to conventional electron spectroscopy, employing a hemispherical electrostatic analyser, a magnetic bottle time-of-flight correlation spectrometer has lower resolving power in particular for high kinetic energy electrons and imposes requirements on the time structure of the radiation source. However, in contrast to the conventional single particle spectroscopy technique, the present method is able to efficiently provide information on electron energy correlations, which opens up the possibility to investigate multi-electron ionisation processes in details.

3.2.4 Set-up augmented with in-line Wiley-McLaren mass spectrometer

The spectrometer set-up discussed above is dedicated to the detection of electrons only. The ionic products practically cannot be detected by this set-up, since they are much heavier and are barely affected by the trapping magnetic field. However, the ions are also interesting to investigate in coincidence with

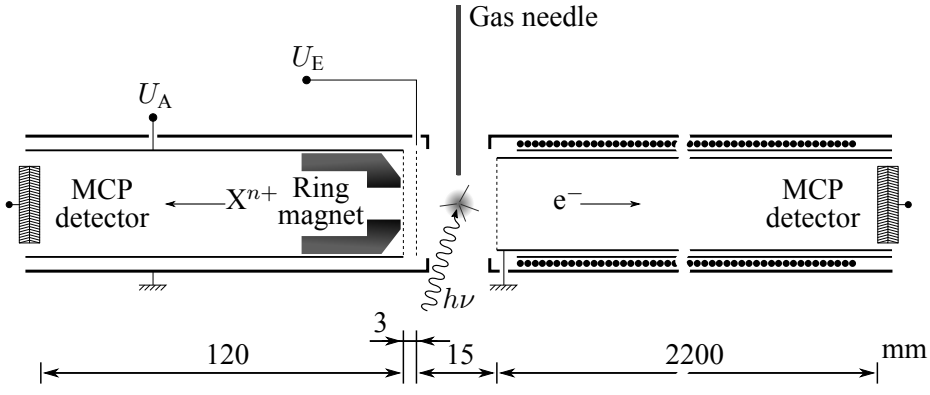

Figure 3.4. Illustration of the electron-ion coincidence set-up which combines a magnetic bottle with an in-line Wiley-McLaren time-of-flight spectrometer.

the electrons particularly in the case of molecules, which may dissociate upon ionisation (see §2.4) and for collecting the information on the final charge state the target species.

In order to investigate the fate of multiply ionised systems, the magnetic bottle instrument has been modified by replacing the conical magnet by an ion time-of-flight spectrometer which contains a hollow ring magnet at the entrance to its flight tube as shown in Figure 3.4. This modification was introduced by John H. D. Eland and Raimund Feifel [8] in 2006. Since the hollow magnet in the original design of this setup is weaker than the conical magnet mentioned before, the gradient of B is smaller and consequently the resolving power of the electron kinetic energy is reduced to about $E/\Delta E \approx 20$.

The ion part is based on a Wiley-McLaren mass spectrometer [37], originally introduced in 1955. It uses pulsed potentials in order to extract and focus the ions essentially without distortion of the electron kinetic energy. In the present set-up, there are two meshes at 3 mm distance between each other on the ion side and one earthed mesh on the electron side. An ion extraction potential U_E of about 300 V is delayed by few hundred nanoseconds after the radiation pulse, allowing the electrons to leave the interaction region, guided by a small (typically less than 1 V) electron extraction potential in addition to the magnetic field. The rest of their motion takes place within the 2.2 m long electron flight tube, which is screened by the third mesh. After the delay, the ions are pushed towards the region in between the two meshes where a constant acceleration potential U_A of about 1 kV is applied. This two stage acceleration focuses the ions before they pass though the ion flight tube. The tube is electrically connected to the second mesh and thus it is on the same high voltage potential, making the ions to travel through a field-free region after the acceleration. An additional advantage of the two-stage acceleration

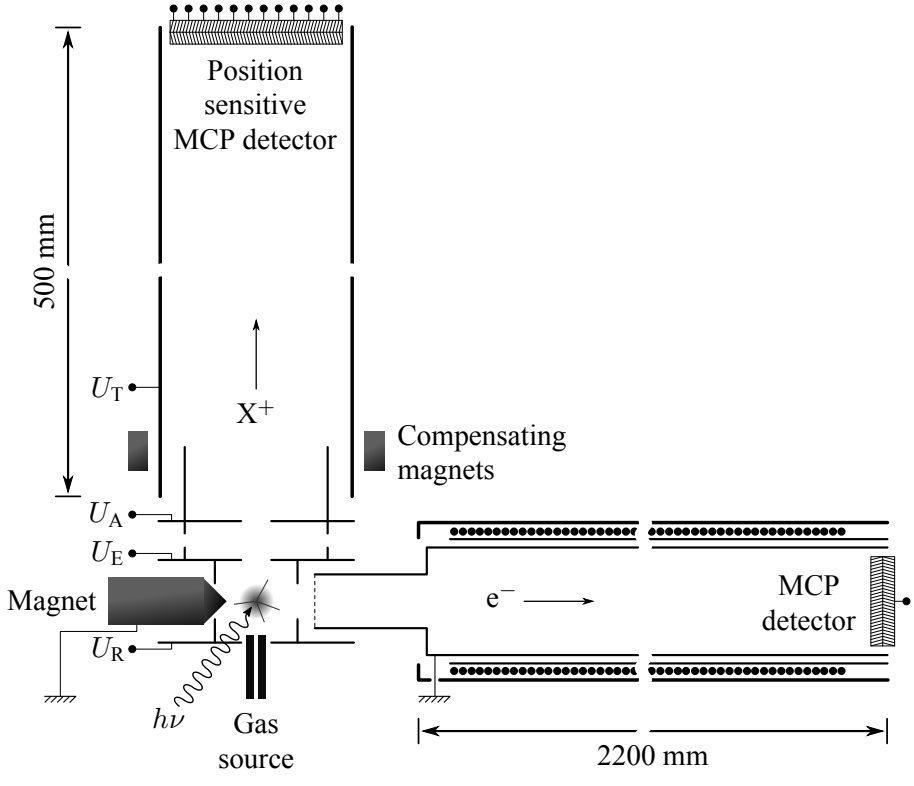

Figure 3.5. Illustration of the electron-ion coincidence set-up with the magnetic bottle and a velocity map imaging time-of-flight spectrometer in perpendicular geometry.

is the possibility not to expose the interaction region to a high voltage. The resolving power for the ion mass is $m/\Delta m \approx 50$.

A disadvantage of grids is reduced collection efficiency of the spectrometer and the likely emission of secondary electrons when hit by photons, ions or other electrons. This can affect the real signal including a substantial increase of the accidental coincidence rate. However, the latter can be excluded during the analysis by selecting only events where at least one ion and one electron were recorded simultaneously. Typical collection efficiencies for this set-up are about 40% for electrons and 10% for ions.

3.2.5 Set-up augmented with perpendicular VMI ion mass spectrometer

An alternative technical solution for combining electron detection in a magnetic bottle and ion detection in a separate spectrometer builds on a perpendicular geometry of the two detection systems, which is illustrated in Figure 3.5 and which was originally devised within the scope of this thesis work as pre-

sented in Paper V. This solution has several advantages compared to the previously described in-line set-up. It allows the use of the same conical magnet as in the electron-only set-up described in §3.2.3, thereby exploiting essentially the full electron kinetic energy resolution of the magnetic bottle, and it allows for an ion detection system with imaging capabilities.

The ion detection system devised for this new set-up is based on the known velocity map imaging (VMI) principle [11]. As can be seen from Figure 3.5, it consists of three electrodes made in the form of flat rings, which are referred to as repeller, extractor and accelerator. The repeller is mounted below the interaction region while the extractor is placed above that region, and the accelerator is implemented at the entrance to the ion flight tube, right above the extractor. While the apertures in the extractor and accelerator are vital to transmit the ions into the tube, the one in the repeller is used in order to introduce the sample gas into the interaction region, here done by using a capillary.

Similar to the previous electron-ion set-up, voltage pulsing is used in order to preserve from disturbance of the electron path while extracting the ions. At the entrance of the electron flight tube a tailor-made extension with a grid is attached, which makes it fit exactly in between the gap of the repeller and extractor, in order to effectively catch the electrons as close as possible to the interaction region. Because of this, the time delay between the radiation pulse and the ion extraction potential can in practice be reduced to few tens of nanoseconds, which is beneficial for catching energetic ion fragments.

In the original velocity map imaging set-up [11] devised for electron detection, the accelerator was earthed and accordingly referred to as ground electrode. In our set-up there are already parts on the electron detection system, which are either earthed or put at very low voltages, in particular the extended electron flight tube and the magnet, which could affect the ion signal. Therefore, the accelerator potential, U_{A}, is nominally set to -5 kV and is pulsed, while the applied voltages on the repeller, U_{R}, and extractor, U_{E} are about $+500$ V and -500 V, respectively. Furthermore, the ion flight tube potential, U_{T}, is constantly kept on the same voltage as the accelerator. The ions are guided first by the extraction potential between the repeller and the extractor and then by a much higher acceleration potential between the extractor and accelerator.

An important part of the velocity map imaging technique is the usage of a position sensitive detector, which in our set-up was a set of micro-channel plates equipped with either a phosphor screen and a charge-coupled device (CCD) camera or a three layer delay-line anode of hexagonal geometry on the back. As the name velocity map imaging implies, this technique delivers information not only on the detector arrival time of the particles, but also on the position where they hit the detector.

The working principle of velocity map imaging can be understood quite easily by considering the case of Coulomb explosion of a doubly charged homonuclear diatomic molecule in its ground state. Before any potentials are applied,

the possible product positions give rise to a sphere which expands in time. When the voltages are applied, the sphere is pushed towards the flight tube and deformed. In the direction perpendicular to the ion flight tube axis, the potentials expand the sphere and the final radius of the sphere in this direction is determined by the total energy gain, mass and initial kinetic energy of the ions. Furthermore, ions of identical mass and charged state emitted at the same angle and with equal initial kinetic energies, but arisen at different positions within the interaction region are focused to the same position on the detector, greatly enhancing the energy resolution.

The ions, emitted in opposite direction to the ion flight tube are accelerated somewhat higher than those which are emitted towards the tube. Therefore in parallel direction the sphere shrinks, which leads to a focusing effect in time. There is a focal distance at which the time-spread is minimised, since the more accelerated ions will eventually overtake those which were ahead in the beginning. The focusing conditions are defined by the ratio between the accelerating and extracting potentials as well as by the ion mass. In practice, the ratio is chosen in order to focus a specific range of masses, which is most interesting in a given experiment, onto the detector plane. The ion position within the resulting circle delivers the information about the initial velocity vector direction, projected onto the detector plate. A hit, detected in the centre of the circle corresponds to ions, emitted toward the detector or in opposite direction. A hit at the edge of the circle means, the ion was emitted perpendicularly to the ion flight tube axis.

Apart from the advantages of this new set-up in comparison of the original in-line set-up already mentioned above, another advantage is the absence of grids on the ion side, which prevents from trajectory deflections, undesired creations of secondary electrons coming off the grids when hit by the primary particles or scattered photons, and from a compromised transmission capacity for ions. A disadvantage of this set-up is the disturbance of the ion trajectories by the permanent magnet on the electron side. In order to counteract this effect we introduced compensating magnets as shown in Figure 3.5.

3.3 Synchrotron radiation

Our set-up benefits from a highly monochromatic VUV or X-ray source at a decent photon flux. This can be achieved by using *synchrotron radiation*, which in accordance to the Maxwell equations is emitted by accelerating charged particles.

The central part of a synchrotron radiation facility, such as BESSY II in Berlin, is the *storage ring*. It consists of a number of straight sections interconnected with bending magnets into a polygon. Ultra high vacuum is essential in order to keep electrons in the ring in cycling motion for a period of several hours. Electrons orbiting in the ring are accelerated to a relativistic velocity.

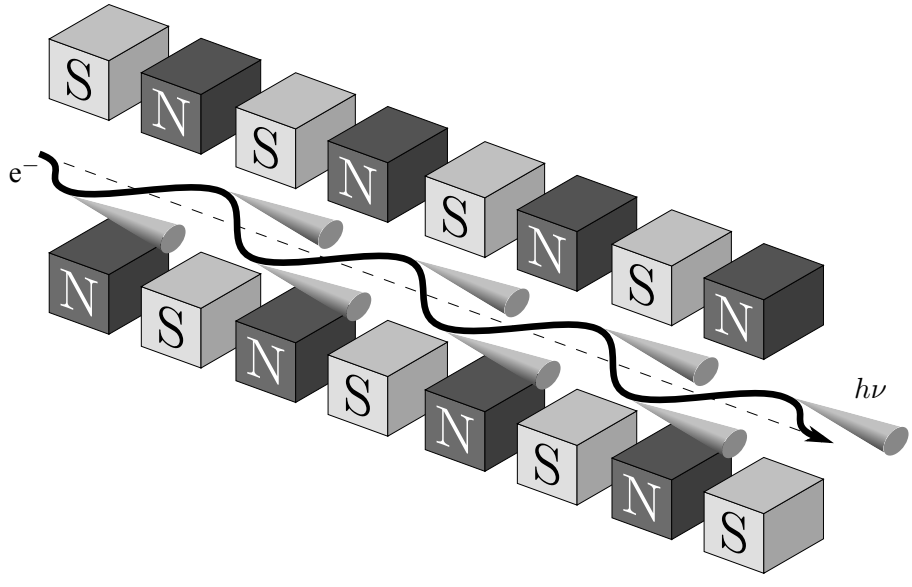

Figure 3.6. Illustration of an undulator.

At BESSY II the circumference of the ring is 240 m and, accordingly, the cycle period of electrons is 800.5 ns.

Insertion devices are placed in the straight sections of the storage ring. Most of the experimental work presented in this thesis has been performed utilising an *undulator*, which is schematically shown in Figure 3.6. The undulator imposes a magnetic field, which is static in time, but periodical along the velocity vector of the electrons. In this design the Lorentz force deflects electrons away from and back to the main axis resulting in nearly sinusoidal trajectory and the emission of synchrotron radiation. Because of the relativistic length contraction, synchrotron radiation is emitted in a narrow cone among the axis. Most of the emission takes place at the furthest off-axis points of the trajectory, where electron acceleration reaches its maximum. The magnetic field strength is chosen in order to let the radiation cones from different parts of the trajectory intersect each other and therefore interfere. The constructive interference can occur for those wavelengths, which are integer times smaller than the delay between the emitted radiation and the electrons per one undulator period. Those wavelengths can be chosen by a comparatively small change in the magnetic field magnitude, which depend on the gap between the top and bottom magnet arrays.The radiation from the undulator then has a line spectrum. It is not affected by the next bending magnet and continues to propagate tangentially to the ring into a so-called *beamline.*

The principal component of a beamline is a monochromator, which employs diffraction in order to select one particular photon energy from the undulator spectrum. The monochromator resolution is $\Delta E < 300$ meV.

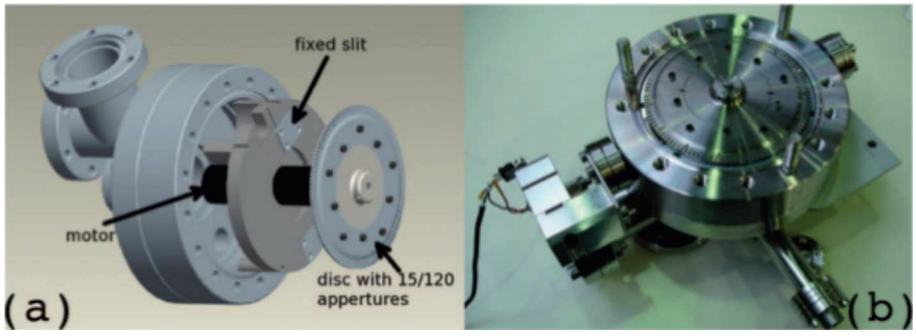

Figure 3.7. Drawing (a) and photo (b) of the chopper. Taken from [39]. Rights belong to respective athors.

The beamlines U49/2 PGM-1 or U49/2 PGM-2 [38] utilising the same undulator at BESSY II in Berlin have been used for almost all the experimental work presented in this thesis. At these beamlines the photon energy can be tuned in the range of 85–1600 eV.

The electrons orbiting in the ring are not continuously distributed, but agglomerated into groups, called bunches. There are several operational modes of a storage ring. The experiment described in this thesis require single bunch mode, usually available at BESSY II only 3 weeks per year. In this mode there is only one bunch of electrons in the ring, therefore the undulator generates a pulse every 800.5 ns. A typical length of the pulse is 30 ps.

3.4 Chopper

The flight time of near zero energy electrons and the heaviest ions which can be detected by our instrument is typically few to several microseconds, while the time spacing between the pulses at the BESSY II storage ring in single bunch mode is only 800.5 ns. Because of this, it is challenging to unambiguously attribute particles to a particular ionising radiation pulse with the spectrometer directly connected to the beamline.

A practical solution of this problem is to exclude some of the radiation pulses by adding a mechanical chopper in between the beam line and the spectrometer. A synchronous chopper for the present apparatus was developed by the collaborating research groups of Hans Siegbahn and Raimund Feifel [39] in 2012 and is shown in Figure 3.7. It is based on two coaxial discs with two arrays of slits: the outer has 120 slits and the inner array consists of 15 slits. By displacing the discs relative to each other, it is possible to tune the effective width of the slits and hence the opening time of this chopper.

The discs are driven by an electromotor, which is phase-locked to the radio frequency signal of the storage ring. The chopper chamber also comprises a 40 μs fixed slit which can be positioned in line with both slit arrays and placed

in the focus of the beamline. Once the chopper is synchronised to the radio frequency signal of the storage ring, it can efficiently filter pulses to let through to the interaction region of the spectrometer only a fraction of them. The most common mode of operation uses an array of 120 slits at a rotational frequency of the discs of about 650 Hz, which raises the inter pulse period to about 12 μs. This is usually more than enough for both electrons and ions to make their way towards the detectors.

4. Data analysis

4.1 Time-to-energy conversion and calibration

The data recorded with the spectrometer discussed in previous chapter is obtained in its raw form in the time domain and represents the time difference between the time reference signal from the radiation source and the time when a particle hits the detector as registered by our acquisition system. While the time-of-flight data for ions can typically be handled and understood fairly easily, this is usually not the case for the electron data. Thus, it is beneficial to convert the electron flight time information to the kinetic energy domain.

Using the energy conservation law, we can represent the initial kinetic energy E_{kin} of the registered electron as

$$E_{\text{kin}} = \frac{mv^2}{2} + E_0 = \frac{ml^2}{2(t - t_0)^2} + E_0 \tag{4.1}$$

where m is the electron mass, v is the magnitude of its velocity, E_0 represents the electrostatic field in the interaction region, either induced or imposed intentionally, t is the recorded flight time, t_0 is the offset between the reference signal and the actual radiation pulse, and l is the length of the electron trajectory. Introducing the constant $D = ml^2/2$, we can rewrite this equation as

$$E_{\text{kin}} = \frac{D^2}{(t - t_0)^2} + E_0 \tag{4.2}$$

which has been used in practice for the time-to-energy conversion during the analysis in the present work. D, t_0 and E_0 are calibration parameters and need to be determined. D is related to the length of the electron trajectories, and t_0 is determined by the time difference between the start of the measurement and the arrival of radiation pulse. These two parameters stay essentially unchanged upon changing the sample. The third parameter E_0 is determined by electrostatic potentials in the interaction region. This parameter sometimes changes with the sample due to changes in surface potentials, which may get affected by the sample.

In order to establish the calibration parameters, additional short experimental runs are carried out ideally before and after the main experiment with the same settings, using a sample, most often a noble gas, with well-known ionisation energy value. For instance, in Papers I and II Argon photoelectron

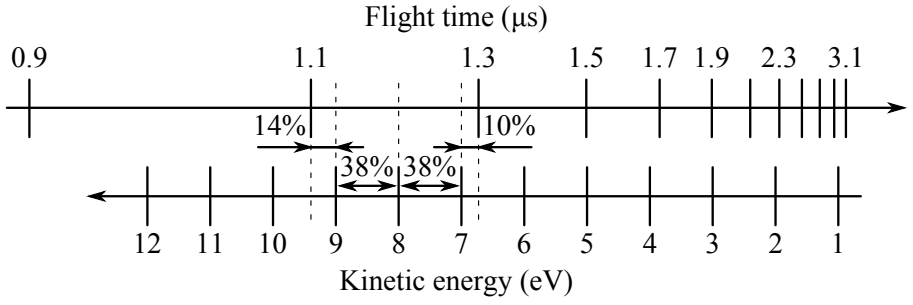

Figure 4.1. Illustration of the relation between the time and energy domains with constant bin sizes of 0.2 ns and 1 eV respectively. An intensity redistribution procedure applied to 1.1–1.3 ns time bin is shown.

spectra have been recorded at 13 photon energies in the interval 251–355 eV. They reveal pairs of peaks corresponding to spin-orbit splitted $2p_{1/2}$ and $2p_{3/2}$ photoelectron lines with ionisation energies of 248.623 eV and 250.77 eV respectively [40]. Subtracted from the photon energies, they deliver 26 values of kinetic energy, which are related to their flight times extracted from the spectra. In order to calculate the calibration parameters, a least square regression based on Equation (4.2) has been applied to these data points. In the particular case of the data used in Papers I and II, the best fit resulted in: $D^2 \approx 60.9$ eV$\times$ns^2, $t_0 \approx -209$ ns, $E_0 \approx -1.29$ eV.

4.2 Non-linearity of the conversion

The raw experimental data in the time domain are obtained with a specific sampling rate, which in the present work was either 1 or 10 GHz. This defines the smallest step in time, called *bin,* which in the present work was either 1 or 0.1 ns. Every detected particle gets a time value corresponding to the centre of the bin closest in time. Subsequently, if the time scale is simply converted to the energy domain, the resulting energy bin size is non-constant and increases towards the higher kinetic energy end in accordance with Equation (4.2). This distorts the intensity information in the spectrum, since a definite integral over more than one bin is not proportional to the particle counts.

As a specific example, we can consider the valence single ionisation spectrum of acetaldehyde, taken at the photon energy of 21.22 eV, which corresponds to the $2p \rightarrow 1s$ transition in Helium. According to the literature [41–45], the spectrum is expected to fall within the kinetic energy range of 0–12 eV. However, we exclude values below 1 eV, because this range corresponds to a large amount of time bins and thus, uncorrelated background counts affects the real signal quite strongly. Furthermore, for the sake of simplicity, we define an abnormally high bin size of 1 eV and thus, only 11 bins in total as shown in Figure 4.1. We also enlarge the bin on the time scale by combining several

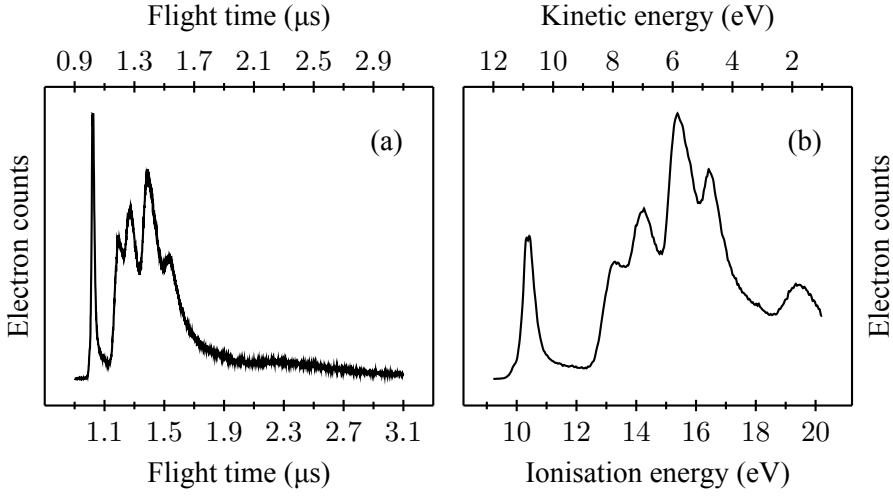

Figure 4.2. Single photoionisation electron spectrum of acetaldehyde measured at the photon energy of 21.22 eV, presented in time (a) and energy (b) domain. Both kinetic and ionisation energy scales are shown.

bins into one. The size of 0.2 μs provides the same number of bins in both domains within the range, corresponding to 1–12 eV as shown in the upper part of the figure.

In order to properly convert the intensity information with the defined constant energy bin, the counts from each time bin are redistributed according to the overlap between the time and energy bins. This is illustrated in Figure 4.1 for the bins between 1.1 and 1.3 μs. Since it fully includes two energy bins between 7 and 8 and between 8 and 9 eV, they get the same fraction of the total counts from the time bin, namely 38% each. There are two other energy bins, one between 6 and 7 and another one between 9 and 10 eV, which only partially overlap with the time bin in point at a fraction of the total length (in energy scale) of about 10% and 14%, respectively. They obtain the corresponding fractions of the total counts of the time bin. However, it should be noted, that additionally both of them also receive contributions from the neighbouring time bins. Applying the procedure described to each time bin, we derive a spectrum based on a constant bin size on the kinetic energy scale. Finally, using Equation (2.2) for single ionisation, we can convert the spectrum to the ionisation energy scale.

In actual analysis, the time bin size is kept the same as in the raw time-of-flight data, while the energy bin size is chosen based on the experimental resolution, i.e. it should be small enough in order to represent all the resolved spectral features, but suitably large in respect to the statistical noise. Figure 4.2(a) shows the sample spectrum discussed above on the time scale with a bin size of 1 ns and Figure 4.2(b) represents the same spectrum converted to the energy

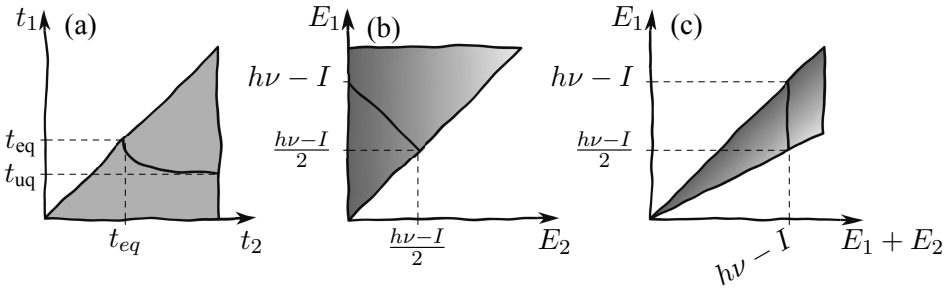

Figure 4.3. Illustrations of features on coincidence maps representing the direct double ionisation process for a single final dicationic state. (a) flight time scales on both axes; (b) kinetic energy scales on both axes; (c) kinetic energy of the fastest electron versus the sum of the kinetic energies of both electrons. $t_{1,2}$ and $E_{1,2}$ denote flight time and kinetic energy of the first and second arrival electron, I is double ionisation energy, $h\nu$ is photon energy, t_{eq} is flight time for the case of equal energy sharing for both electrons; t_{uq} is flight time of the first arrival electron in the case of the most unequal sharing. Colour gradient shows the distribution of uncorrelated background.

domain using the procedure described with a bin size of 40 meV. In addition to the kinetic energy scale, the ionisation energy scale derived according to Equation (2.2) is included.

4.3 Correlated multi-particle data and coincidence maps

Correlated data can be expressed as a multidimensional function, where arguments are flight time values of all particles or energies of electrons within every multifold coincidence event, while the function represents the coincidence counts. In what follows, we assume the analysis of a direct double photoionisation process described in §2.3. A conventional way for representing three-dimensional coincidence data in two dimensions are *coincidence maps*. An example of different coincidence maps are schematically shown in Figure 4.3. The numerical indexes denote the order of detection of the electrons, that is t_1 and E_1 correspond to the flight time and kinetic energy of the first arrived (faster or more energetic) electron and t_2 and E_2 represent the corresponding values for the second arrived (slower or less energetic) electron.

In the first map, Figure 4.3(a), electron pairs are represented on the raw time-of-flight scale. In this case, the electron pairs, corresponding to a particular doubly ionised state constitute a hyperbolic section. The time value labelled as t_{eq} on both axes corresponds to an equal energy distribution between two electrons, therefore their flight times are also identical. Using this value, it is possible to derive the energies of the electrons, corresponding to the energy $(h\nu - I)/2$, thus the ionisation energy can be estimated. The other end of the curve is associated with the opposite situation, where the faster electron of

the pair receives essentially the whole available excess energy. The respective flight time t_{uq} of this electron can also be used in order to estimate the ionisation energy, since it corresponds to the energy $h\nu - I$. However, this way of deriving I is not practical, since in this area there is often only a small part of the full direct double ionisation statistics, which can be used. Furthermore, pairs corresponding to either t_{eq} or t_{uq} are not observed in actual experiments. The first one implies that both electrons arrive simultaneously to the detector. Such electrons are difficult to observe with single MCP detector due to the fact, that the electronics are not able to discriminate two exactly simultaneous signals as two separate particles. Moreover, in practice even an electron arriving some nanoseconds up to few tens of nanoseconds after the previous one may not be registered due to signal ringing in the detector after the first hit. The examination of the second energy t_{uq}, corresponding to an unequal distribution is also challenging, because near zero-energy electrons overlap with the background, which contributes more at longer flight times.

The second map in Figure 4.3(b) depicts the same imaginary data, but converted to the energy domain using Equation (4.2) for both electrons. Since the energy sum of both electrons involved in the process is constant for a given dicationic final state, the respective electron pairs constitute a straight antidiagonal line segment. Akin to the previous case, the end points of this segment correspond to the most equal and unequal energy distributions and relate to the ionisation energy as $(h\nu - I)/2$ and $h\nu - I$, respectively. Using this map, it is possible to include more easily the complete statistics for a given final state by applying a linear least-square regression to the segment. However, it does not allow us to determine so easily the width and the form of the corresponding peak on the double ionisation energy scale and therefore the profile of the double ionisation spectrum based on such a map.

One can also represent the data in another form of coincidence map, which has the excess energy, that is the energy sum of both electrons, on one of the axes. Such a map is shown in Figure 4.3(c). The line section, corresponding to a particular dicationic final state formed by the direct double ionisation process is perpendicular to the excess energy axis. Such a coincidence map can finally lead us to the double ionisation spectrum. In order to derive this spectrum, we integrate along the axis associated with the energy of one of the electrons (in this case the fastest electron) or, in other words, project the map onto the excess energy axis. As a final step, we use the known photon energy value and the Equation (2.4) to convert the excess energy scale to the double ionisation energy scale. Since the last transformation is linear, it does change the bin size and thus does not require any further work on the intensity information.

Very similar approaches are taken when working with direct triple ionisation data and possibly direct multifold ionisation of higher levels, but in these cases there are more dimensions involved and therefore the intermediate data are not so easy to display.

Another type of double ionisation process is normal Auger decay. As it is explained in §2.2, the firstly emitted electron corresponds to single core ionisation, while the energy of the secondly emitted electron is defined by the doubly valence ionised final state. In all three representations of the coincidence data, described above, a given final state would correspond to two very well defined energies forming a dot on coincidence map. However, often there is no need to represent the Auger data in form of a coincidence map. Instead, we can use the core electron in order to select electron pairs, where one is attributed to the core level of interest and then work with the data of the other electron as two-dimensional data. The double ionisation scale is then derived according to the linear Equation (2.3) using the value for single core ionisation, usually known from the literature, e.g. Ref. [6].

Coincidence maps are also useful in the analysis of data including ionic fragments upon dissociation of molecules. The flight times of ions detected in pairs can be represented as a coincidence map, where spots corresponds to different fragmentation patterns. As an example in Paper III such a map obtained by selection on different electron lines provides the information on how the relative probabilities of patterns depend on the initial photoionisation step. The shape of the spots may reveal the information on fragmentation dynamics [46].

5. Results

5.1 Acetaldehyde (ethanal)

5.1.1 Double valence photoionisation

At photon energies substantially below the 1s ionisation threshold of acetaldehyde, which corresponds to the methylic C1s line at 291.80 eV [47], primarily valence levels will contribute their electrons to the ionisation processes. Therefore, upon selection of electron pairs created at the photon energies of 40.8 and 95 eV only double valence ionisation is expected. Following the procedure explained in §4.3, the left panel of Figure 5.1 represents the electron pairs obtained at the photon energy of 95 eV as a coincidence map with kinetic energy of one electron versus another, akin to the representation of Figure 4.3(b). The series of antidiagonal line segments visible on the map is attributed the to direct double valence ionisation process of acetaldehyde. Each segment corresponds to some fixed excess energy value and therefore to a fixed ionisation energy. Other notable features include two sets of higher intensity spots corresponding to the case where one of the electrons in pair has a kinetic energy of about 25.5 eV and 27.5 eV, respectively. They are attributed to the ionisation of $4d_{3/2}$ and $4d_{5/2}$ electrons of Xenon [48], residual from the previous optimisation work on the spectrometer and all the spots belong to subsequent Auger decay channels. Also as the horizontal projection above the map shows that, the intensity increases for the slower electron approaching zero kinetic energy, which is attributed to an enhanced contribution from the background due to the fact that large flight time intervals correspond to very short energy ranges, thus the uncorrelated background closer to zero kinetic energy affects the spectrum more severely.

By shifting each bin in the map horizontally with the corresponding value for the kinetic energy of the slower electron, we transform the horizontal axis to the energy sum scale, which is shown in the right panel of Figure 5.1. After this transformation, the line segments attributed to double valence ionisation are vertical and the projection onto the horizontal axis represents the populations of different ionisation paths through involvement of particular pairs of valence electrons. The Xenon contamination does not significantly affect the profile.

By subtracting the kinetic energy sum of two electrons, as determined in the analysis above, from the photon energy in accordance to Equation (2.4), we can derive the double ionisation spectra of acetaldehyde which are shown in Figure 5.2 for the photon energies of 40.8 and 95 eV. These spectra represent the population of the dicationic states upon direct double valence ionisation.

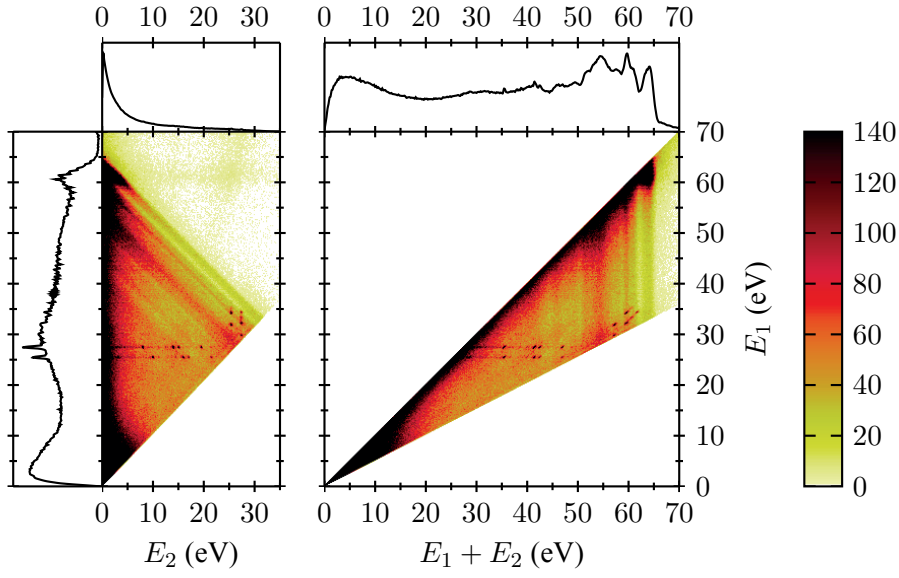

Figure 5.1. Coincidence map of electron pairs in acetaldehyde, measured at the photon energy of 95 eV. E_1 is the energy of the faster electron and E_2 is the energy of the slower electron. The dots reflect reflect the presence of residual Xenon. Plots above and to the left of the maps correspond to projections of the maps onto different axes. Colour indicates the counts per bin. The bin size is 0.2 eV.

For comparison a normal Auger spectrum following $O1s^{-1}$ ionisation of acetaldehyde adopted from the work by Correia *et al.* [47] is also included. This spectrum has been obtained by combining two measurements using a hemispherical electrostatic analyser with different resolution settings and an X-ray source at the photon energy of 1487 eV, which corresponds to the $2p_{3/2} \rightarrow 1s$ transition in aluminium [6].

A clear correspondence between the peak positions in both valence double ionisation and the $O1s^{-1}$ Auger spectrum is visible in Figure 5.2. This is due to the fact that the dicationic final states are expected to be the same in both cases. However, their relative populations are different because of the different nature of the processes leading to these states. The onset at double ionisation energy of about 29 eV in all spectra corresponds to the lowest double ionisation threshold.

The $O1s^{-1}$ Auger spectrum of acetaldehyde was assigned by Minelli *et al.*, [49], which allows us to use this assignment for the characterisation of the valence double ionisation process. It should be noted that the Auger decay populates mainly singlet states while in double valence ionisation it is expected that singles and triples are enhanced similarly, though according to calculations [47, 49], the singlet-triplet splitting is small compared to our instrumental resolution. This has been taken into account in the assignment given in Paper I.

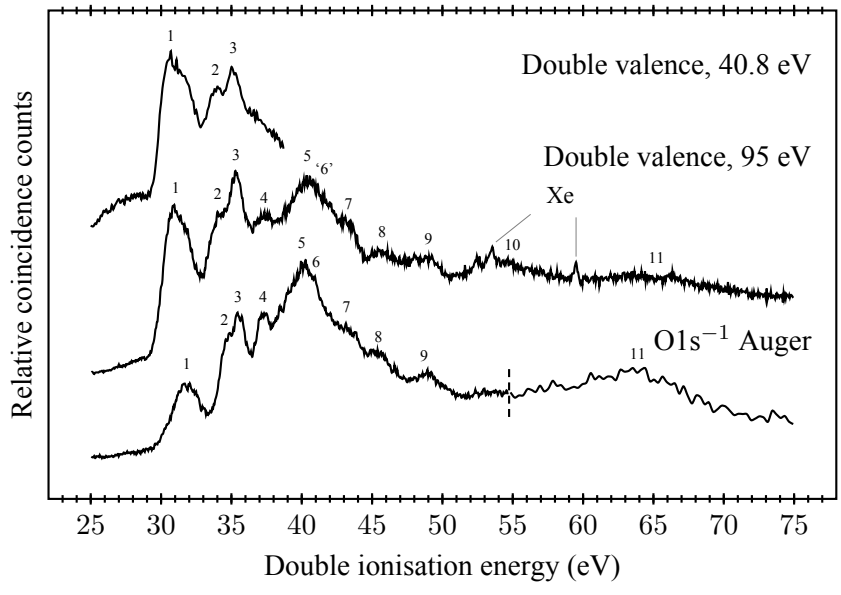

Figure 5.2. Double valence ionisation spectra of acetaldehyde at photon energies of 40.8 and 95 eV from Paper I and for comparison the Auger spectrum upon O1s^{-1} core hole formation in acetaldehyde, adopted from Reference [47]. Features associated with Auger decay from residual Xenon are marked.

5.1.2 Site-specific single Auger decay

Acetaldehyde has two carbon atoms in different chemical environments and according to what was discussed in §3.1, this can lead to a chemical shift between the photoelectron lines associated with the formylic and methylic C1s electrons. According to Correia *et al.* [47] their ionisation energies are 294.45 eV and 291.80 eV, respectively, i.e. the chemical shift is about 2.65 eV. This property combined with coincidence spectroscopy can be used in order to disentangle Auger decays upon the formation of different C1s^{-1} core holes in acetaldehyde, which previously [47] were measured only in superposition. Paper I presents these first observations of site-specific Auger decay of acetaldehyde.

In order to derive such site-specific C1s^{-1} Auger spectra, the experimental run for acetaldehyde at 350 eV has been used. This photon energy is well-above both the C1s^{-1} ionisation energies, but still allows us to resolve two lines. Then electron pairs, where the slower electron has an ionisation energy corresponding to either of the two peaks, are selected. The faster electrons from such pairs are employed for the derivation of either of two the C1s^{-1} Auger spectra in the time domain. Then the spectra are converted to the kinetic energy scale as explained in §4.1 and, finally, to the ionisation energy scale according to Equation (2.3). The resulting C1s^{-1} Auger spectra are presented in Figure 5.3 and labelled as “experiment”. In 1995 Minelli *et al.* [49] performed

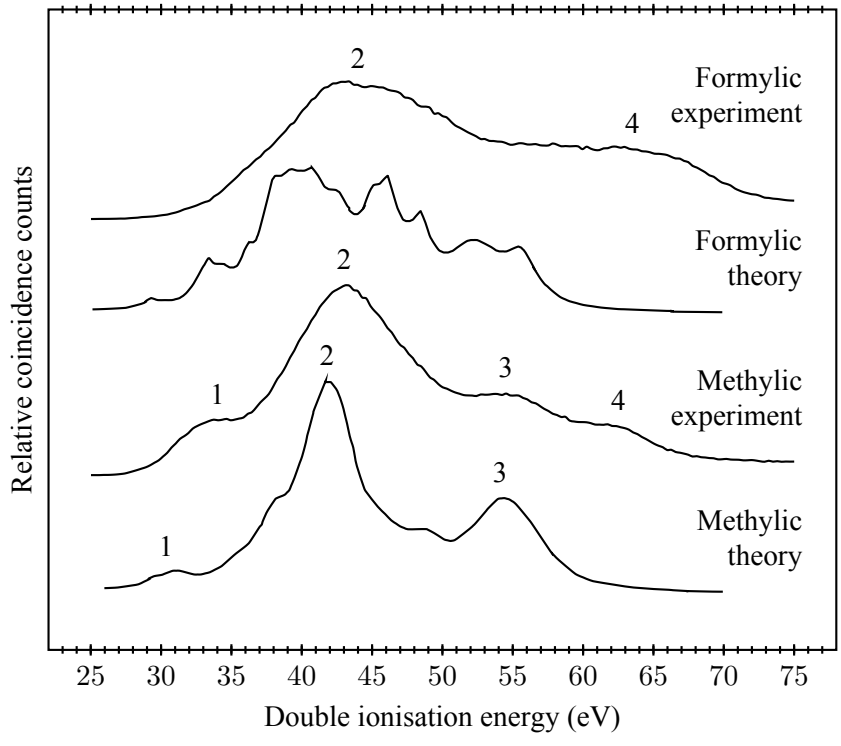

Figure 5.3. Site-specific $C1s^{-1}$ Auger electron spectra of acetaldehyde, measured at the photon energy of 350 eV. Theoretical predictions are adopted from [49] and were included for comparison.

calculations, which predicted the profiles of the two site-specific $C1s^{-1}$ Auger spectra of acetaldehyde shown in Figure 5.3, where they are labelled "theory".

As can be seen from Figure 5.3, the two experimental Auger spectra are quite distinct from each other, demonstrating the signature of site-specificity in the Auger decay. Such an effect is not unexpected for acetaldehyde, since very similar properties were found in the case of acetone [31], a substance related to acetaldehyde, having an additional methylic group instead of the hydrogen atom bound to the formylic carbon.

When comparing the experimental and theoretical data, one needs to take into account that the theoretical curves were modelled with the resolution of the hemispherical electrostatic analyser used in the work by Correia *et al.* [47]. Since the kinetic energy range for the $C1s^{-1}$ Auger electrons is about 220–270 eV, the resolution of the magnetic bottle used in this experiment is about 5 eV for this range. Thus the experimental spectra are not expected to reproduce the fine structure predicted by the calculations. However, the correspondence between the gross features allows us to assign those labelled 1–3

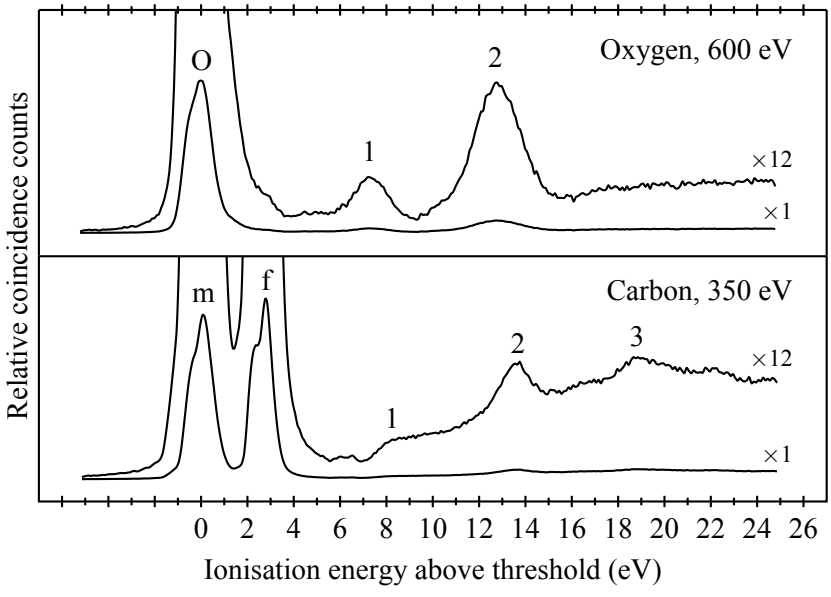

Figure 5.4. Core photoelectron spectra of acetaldehyde with shake-up satellite structures for O1s (upper panel) and C1s (lower panel) ionisation. The horizontal scale shows the single ionisation energy relative to the lowest core hole of each type. Both spectra are provided with two different intensity scales in order to bring out the satellite peaks as well as the main core ionisation structures. Labels "O", "m" and "f" denote O1s, methylic C1s and formylic C1s photoelectron lines, accordingly. The shake-up structures are labelled.

as discussed in Paper I. Higher energy states were not calculated by Minelli *et al.*, therefore feature 4 has so far no interpretation.

5.1.3 Auger decay of shake-up states

Figure 5.4 shows the $O1s^{-1}$ and $C1s^{-1}$ photoelectron spectra acquired at the photon energies of 600 eV and 350 eV. The ionisation energy is given above the oxygen and methylic carbon core levels, respectively. Apart from the main peaks, there are much weaker satellite structures at higher ionisation energies, visible in the enlarged spectra. They are associated with shake-up processes involving the oxygen and carbon 1s levels, respectively, i.e. simultaneous ionisation of a core electron and excitation of another electron. The energy contributed to the excitation corresponds to the shift between the main and shake-up peaks and is called *shake-up energy*.

The satellite structures of acetaldehyde were studied and assigned by Keane et al. [45] in 1991. In expanding on the worth of this work, the fate of these core-ionised and excited states were revealed of Paper I. Akin to the previous

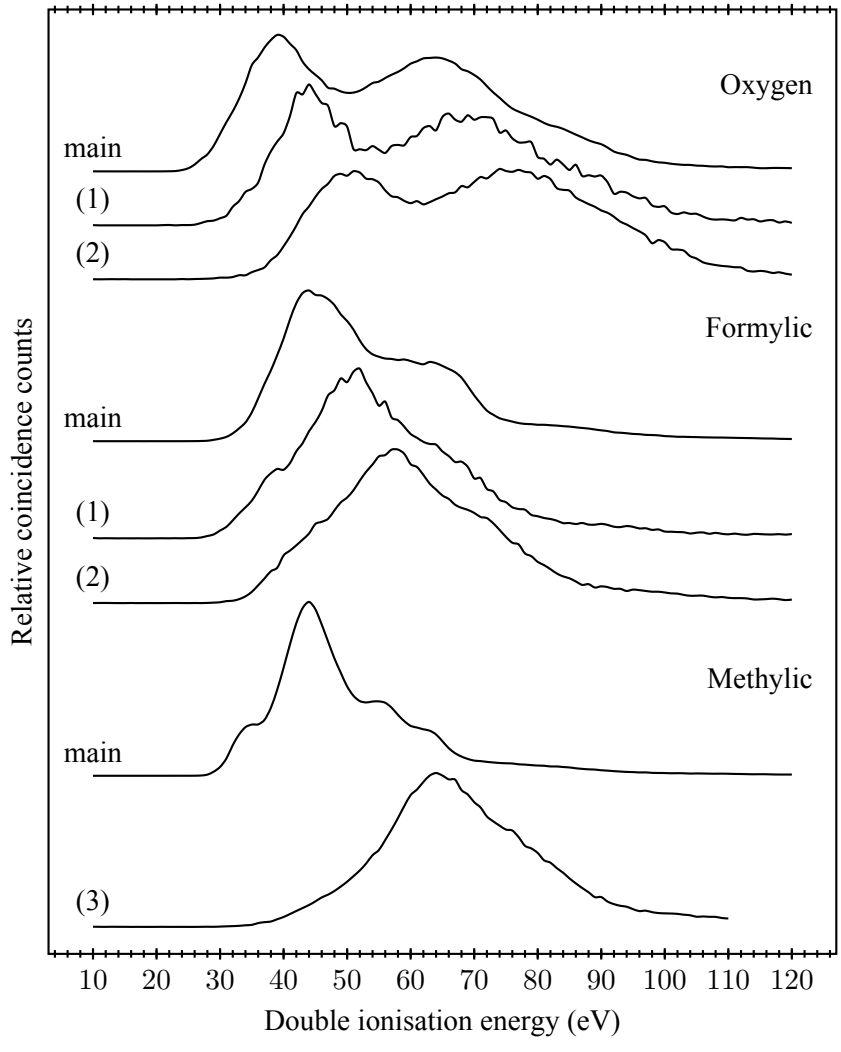

Figure 5.5. Auger decay of shake-up states in acetaldehyde obtained from coincidences with different 1s orbitals. The photon energy is 600 eV for the O1s cases and 350 eV for the C1s cases.

subsection the Auger spectra are derived by selecting on the slower electron of the pair and plotting the spectrum of the faster electron. This time the selection energy range corresponds to different shake-up satellite peaks as well as to the main peaks for comparison. The core ionisation energy I_c in Equation (2.3), used in order to transform the spectrum to the double ionisation energy scale, includes the shake-up energy as determined by Keane *et al.* [45]. The decays of $O1s^{-1}$ states are based on the data acquired at 600 eV photon energy and the decays of $C1s^{-1}$ states are based on the 350 eV data. These spectra are

shown in Figure 5.5. The labelling of the spectra corresponds to the labelling of the peaks in Figure 5.4.

In all cases, the spectra attributed to the satellites are shifted towards higher ionisation energies and these shifts are approximately equal to the shake-up energies of the corresponding peaks in the core photoelectron spectrum. This demonstrates the dominance of the spectator process, i.e. the excited electron does not actively participate in the Auger decay. However, the shift values for the onsets are smaller, than the rest of the Auger spectra, associated with shake-up states. This can be attributed to a small, but still significant contribution from the involvement of participator Auger processes.

5.1.4 Site-spectific double Auger decay and direct triple valence ionisation

The excess energy released upon the Auger decay of a $1s^{-1}$ core hole can be transfered not only to a single electron, but also to an electron pair. Such an ionisation process is commonly referred to as *double Auger decay* and its spectrum can be derived as follows: at first triple electron events are selected, where the energy of one of the electrons lies within the range of the particular $1s^{-1}$ line and then the remaining electrons are analysed similarily to what was done in the case of double valence ionisation in §5.1.1. Since there are in total three electrons involved, the final states must be triply charged. The triple ionisation energy is derived similar to the single Auger case, that is using Equation (2.3), with E_a being the kinetic energy sum of both Auger electrons.

Due to the same set of final states involved, it is interesting to compare double Auger decay with the triple valence ionisation. The latter was derived similarly to the double valence ionisation as described in §5.1.1, but employing an additional dimension in the coincidence map and utilising Equation (2.5) for the derivation of the triple ionisation energy.

Figure 5.6 shows double Auger spectra extracted site-specifically, which were obtained from the data at 600 eV for the initial charge localised on the oxygen atom and at 350 eV for the case of formylic and methylic $C1s^{-1}$ hole formation, in comparison with the triple valence ionisation spectrum measured at 95 eV. Due to the photon energy chosen, the 95 eV spectrum represents only the lower energy part of the tricationic final states. It contains again some sharp features, which are associated with ionisation processes involving residual Xenon.

In most of the spectra the onset, which corresponds to the triple ionisation threshold, is located around 58 eV, but the $O1s^{-1}$ double Auger spectrum seems to stretch several eVs lower in ionisation energy, which can be a merit of resolution. The $O1s^{-1}$ and methylic $C1s^{-1}$ spectra have some structures, which are labelled with numbers. There are no theoretical calculations which allow us to assign them, but a possible explanation suggested in Paper I is,

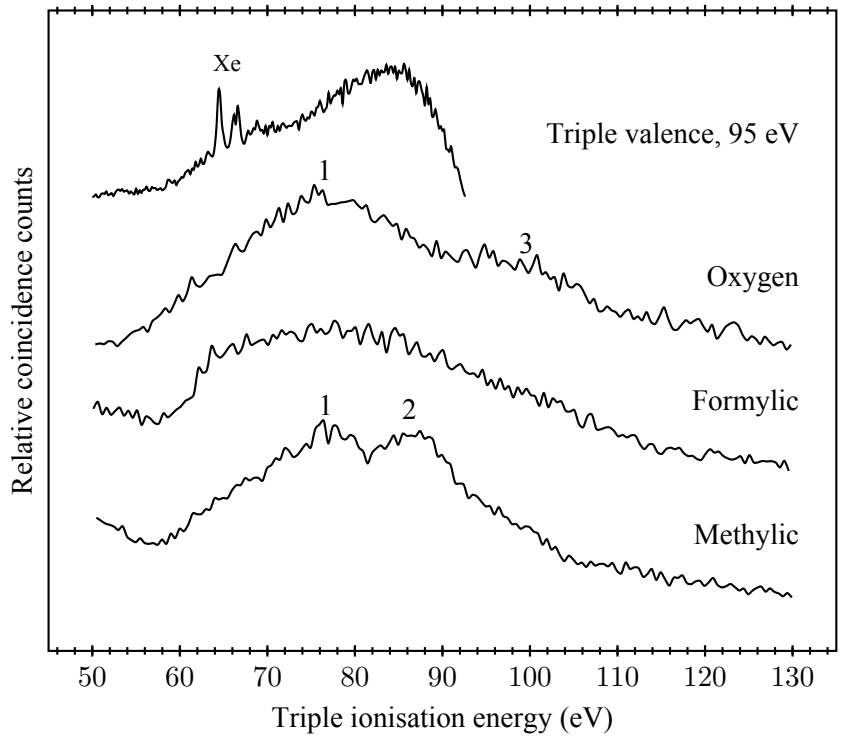

Figure 5.6. Acetaldehyde triple valence ionisation spectrum at 95 eV as well as double Auger spectra at 600 eV (Oxygen 1s) and 350 eV (Formylic and Methylic C1s).

that band 1 corresponds to two of three vacancies in the outermost 10σ orbital, band 2 to one such vacancy, while band 3 mainly resembles the case, where all three vacancies involve deeper shells.

The formylic $C1s^{-1}$ double Auger spectrum and the lower part of the direct triple ionisation spectrum are essentially structureless. The lack of sharp features in all these spectra may be caused by a significantly larger number of possible final states as compared to double and single ionisation as well as by their repulsive nature. Both factors lead to an enhanced overlap between the different states.

5.1.5 Core-valence double ionisation

Direct double ionisation is not only possible for electrons originating from the same shell as was discussed in §5.1.1, but also for different shells. In the case of acetaldehyde at the photon energies above a certain threshold, we can expect to observe direct double ionisation involving an 1s electron and a valence electron. This process is called *core-valence double ionisation*. In the past such processes were investigated for some atomic [36, 50] and small molec-

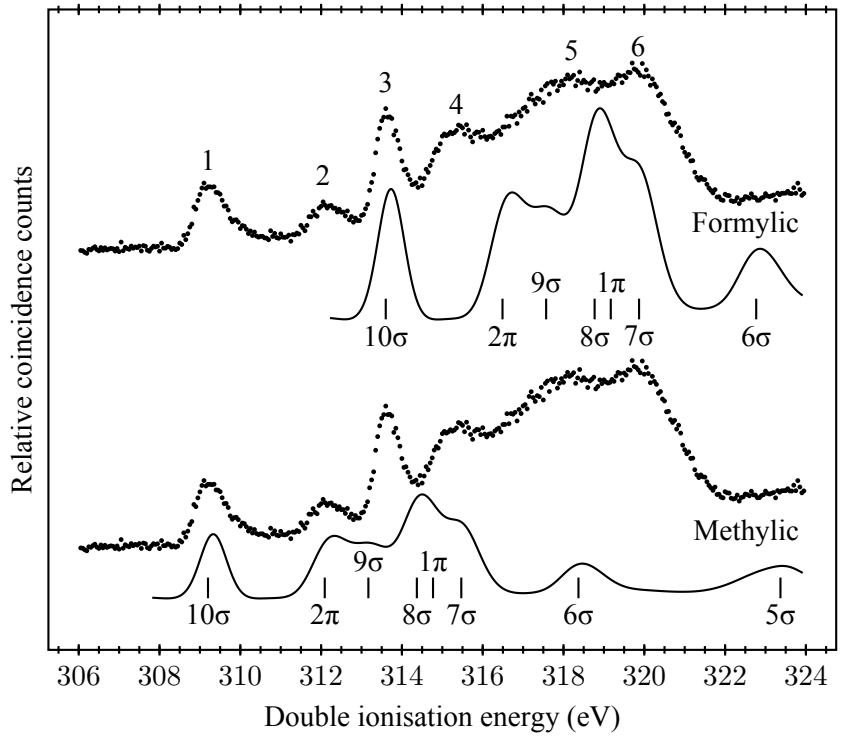

Figure 5.7. Core-valence double ionisation spectra of acetaldehyde involving the formation of $C1s^{-1}v^{-1}$ vacancies at the photon energy of 350 eV shown as dots. The single valence photoelectron spectrum based on the data by Keane *et al.* [45], broadened according to the experimental resolution, is shown for shifts of 303.37 and 298.94 eV in ionisation energy. The labels "Formylic" and "Methylic" denote the C1s orbital thought to be involved in the core-valence ionisation in each case.

ular [36, 51–55] systems. Paper II is exclusively devoted to the core-valence double ionisation of acetaldehyde.

Since two electrons emitted in core-valence double ionisation process share the excess energy in a continuous distribution, there is no specific core peak which could be used for selection. Furthermore, it is not possible to distinguish experimentally which of the two electrons originates from 1s and which from a valence orbital. In the cases of core-valence ionisation involving either of two C1s shells, it also means, that it is impossible to derive site-specific core-valence spectra associated with different carbon atoms of acetaldehyde. Instead, the spectrum includes peaks associated with both formylic and methylic $C1s^{-1}v^{-1}$ states, where v denotes some valence orbital.

In previous works, Andersson *et al.* [52, 53] suggested a simple empirical model to assign the core-valence spectra of molecular oxygen and carbon disulfide based on the known interpretation of the single valence photoelectron spectrum for the same molecule. It assumes that the dominant contribution

from the core shell in comparison to single valence ionisation is the additional energy required to remove the core electron. Based on that, the corresponding single valence photoionisation spectrum was shifted to higher ionisation energies to line-up with the lowest feature of the core-valence spectrum. In the systems investigated by Andersson *et al.* this revealed an impressive one-to-one match between the spectra, leading to the interpretation of the features of the core-valence photoionisation spectrum in terms of $1s^{-1}v^{-1}$ configurations. The assumption above implies that the so-called *core-valence interaction energy*, which is the Coulomb repulsion between the core and valence electrons, is the same for all valence orbitals for a given core orbital.

Figure 5.7 shows the $C1s^{-1}v^{-1}$ core-valence spectrum at the photon energy of 350 eV in dots, which has been derived very similarly to the double valence ionisation spectrum in §5.1.1, based on the data recorded at the photon energy of 350 eV. The single valence ionisation spectrum and its assignment is known from the literature [41–45]. In order to test the above empirical model, for the present case, the single valence photoelectron spectrum measured by Keane *et al.* [45] has been used. In order to take into account the experimental resolution of the spectrometer, this spectrum has been convoluted with a Gaussian function with a full width a half maximum (FWHM) of 0.7 eV. Since the core-valence spectrum is a superposition of processes associated with the formylic or methylic C1s vacancy, we should use the modelled spectrum twice with different shifts.

As one can see from Figure 5.7, the empirical model can possibly suggest an assignment for the first three peaks. Since features 1 and 2 line up with the less shifted single valence ionisation spectrum shown in the lower panel, we can assume that they involve a C1s electron at smaller ionisation energy, which is the methylic one. Peak 3 can then possibly be attributed to vacancies on the formylic C1s level and the outermost 10σ orbital, however it may contain contributions from methylic $C1s^{-1}v^{-1}$ states, too, such as the one involving the 9σ valence orbital.

Figure 5.8 represents the $O1s^{-1}v^{-1}$ core-valence spectrum of acetaldehyde at the photon energy of 600 eV in dots. The same empirical model has been tested here, too. In this case the FWHM of the Gaussian function has been chosen to be 1.4 eV in order to correspond to the expected experimental resolution. As can be seen, the agreement between the core-valence and the shifted double valence ionisation spectrum is insufficient for assignment. This may suggest that there is higher variation of the core-valence interaction energy between the O1s and valence orbitals, than in the C1s case.

In order to better understand core-valence spectra of acetaldehyde a series of quantum chemical calculations using a number of different methods has been performed in order to characterise the experimental core-valence spectra of acetaldehyde. It should be noted here, that such calculations impose a particular challenge: creation of a core hole is associated with substantial relaxation energies and orbital transformations, which is typically handled by a self-consistent

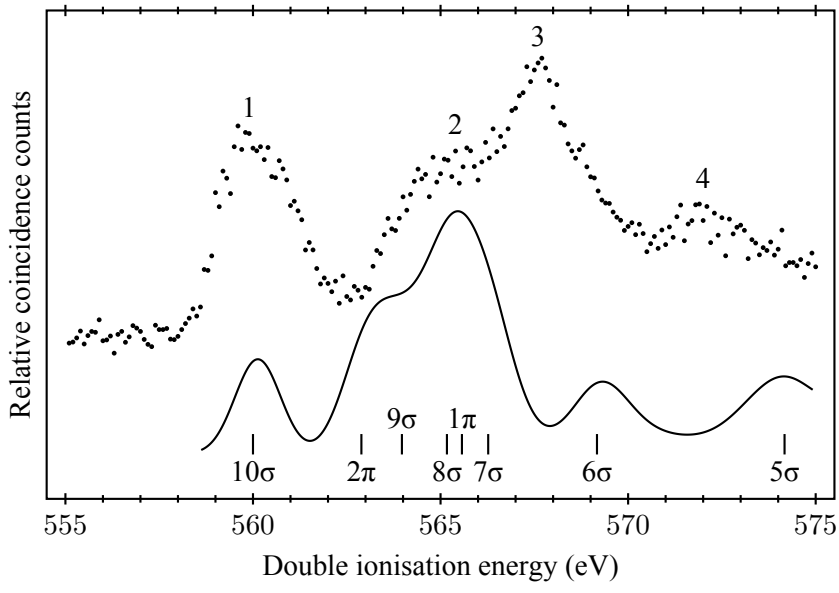

Figure 5.8. Core-valence double ionisation spectrum of acetaldehyde involving the formation of $O1s^{-1}v^{-1}$ vacancies at the photon energy of 600 eV shown as dots. The single valence photoelectron spectrum based on the data by Keane *et al.* [45] broadened according to the experimental resolution is shown with a shift of 549.77 eV in ionisation energy.

field (SCF) procedure. At the same time the involvement of valence orbitals in the ionisation process is best described by perturbational or Green's function theories.

In this work two simple interaction corrected independent particle models, one involving the $Z + 1$ approximation and the other one the Hartree-Fock method, have been tried as well as several more sophisticated correlation methods such as MCSCF (multi-configurational self-consistent field), SDCI (single-double configuration interaction) and CASPT2 (complete active space perturbation theory).

As shown in this study, the $Z + 1$ approximation is able to qualitatively reproduce the lowest part of the $C1s^{-1}v^{-1}$ spectrum, although overestimating the double ionisation energy values by about 2 eV. It suggests, that peak 1 is a superposition of states involving the methylic $C1s^{-1}10\sigma^{-1}$ and $C1s^{-1}2\pi^{-1}$ configurations, and peak 2 is primarily attributed to the methylic $C1s^{-1}9\sigma^{-1}$ configuration, which does not agree with either the empirical model or with other calculations (see below).

In contrast to the approach based on the $Z + 1$ approximation, the results based on the Hartree-Fock model are shifted towards lower double ionisation energies. Furthermore, this method can reproduce the form of the spectrum better and assigns the first three peaks in agreement with the empirical model,

suggesting, that the third peak is a mixture of states involving the formylic $C1s^{-1}10\sigma^{-1}$ and methylic $C1s^{-1}9\sigma^{-1}$ configurations.

MCSCF, considered in the present context as a comparatively low level correlation method, maps qualitatively all the peaks on the experimental $C1s^{-1}v^{-1}$ spectrum. It also mainly supports the interpretation of the low part of the spectrum given by the empirical model. In addition, it suggests for peak 4 key contributions from states associated with the formylic $C1s^{-1}2\pi^{-1}$ configuration. However, states associated with the methylic $C1s^{-1}9\sigma^{-1}$ configuration are found by this method to be located somewhere in between peaks 3 and 4.

The results based on the SDCI calculations for the $C1s^{-1}v^{-1}$ case are very similar to the MCSCF results apart from the fact that they underestimate the double ionisation energies to a lesser degree and that they result in a more reasonable position of the states associated with the methylic $C1s^{-1}9\sigma^{-1}$ configuration, which are suggested to contribute to peak 3 together with the lowest

Table 5.1. *Assignment of the core-valence spectra of acetaldehyde shown in Figures 5.7 and 5.8 based on SDCI calculations discussed in Paper II, except for peak 4 of the $O1s^{-1}v^{-1}$ case, where the assignment is based on the $Z+1$ and Hartree-Fock calculations. The left panel refers to features observed in the spectrum recorded above the C1s ionisation thresholds and the right panel refers to features observed in the spectrum recorded above the O1s threshold. Symbol * denotes the configuration mixed with the $2\pi \rightarrow 3\pi$ excitation (shake-up).*

Carbon, 350 eV		Oxygen, 600 eV	
Feature	Assignment	Feature	Assignment
1	$^{1,3}A'$ $C_m1s^{-1}10\sigma^{-1}$	1	$^{1,3}A'$ $O1s^{-1}10\sigma^{-1}$
			$^{1,3}A''$ $O1s^{-1}2\pi^{-1}$
2	$^{1,3}A''$ $C_m1s^{-1}2\pi^{-1}$		$^{1,3}A'$ $O1s^{-1}9\sigma^{-1}$
3	$^{1,3}A'$ $C_m1s^{-1}9\sigma^{-1}$	2	$^{1,3}A'$ $O1s^{-1}8\sigma^{-1}$
	$^{1,3}A'$ $C_f1s^{-1}10\sigma^{-1}$		$^{3}A''$ $O1s^{-1}1\pi^{-1}$
4	$^{1,3}A''$ $C_f1s^{-1}2\pi^{-1}$	3	$^{1,3}A'$ $O1s^{-1}7\sigma^{-1}$
	$^{1,3}A'$ $C_m1s^{-1}8\sigma^{-1}$		$^{1}A''$ $O1s^{-1}1\pi^{-1}$
	$^{1,3}A'$ $C_f1s^{-1}9\sigma^{-1}$		$^{3}A'$ $O1s^{-1}6\sigma^{-1}$
5	$^{1,3}A''$ $C_m1s^{-1}1\pi^{-1}$	4	$^{1,3}A'$ $O1s^{-1}5\sigma^{-1}$
	$^{1,3}A'$ $C_m1s^{-1}7\sigma^{-1}$		
	$^{3}A''$ $C_f1s^{-1}1\pi^{-1}$		
6	$^{1,3}A''$ $C_f1s^{-1}1\pi^{-1}$		
	$^{1,3}A'$ $C_f1s^{-1}8\sigma^{-1}$		
	$^{1,3}A'$ $C_m1s^{-1}6\sigma^{-1}$		
	$^{3}A'$ $C_m1s^{-1}10\sigma*^{-1}$		
	$^{3}A'$ $C_f1s^{-1}7\sigma^{-1}$		

states of formylic origin. SDCI seems to result in the best overall resemblance with the experimental profile.

Finally the $C1s^{-1}v^{-1}$ results of CASPT2, the most sophisticated methods among the ones tested, basically agree with the $C1s^{-1}v^{-1}$ results of SDCI, but the roots are more significantly shifted towards lower double ionisation energies.

In the case of $O1s^{-1}v^{-1}$ all the methods, except for MCSCF, agree on the contributions to peak 1 from the states with valence vacancies in 10σ, 2πor 9σ. The $Z+1$ and Hartree-Fock methods also suggest to interpret feature 4 as involving the 5σ orbital. The best resemblance in the overall form is, again, provided by the SDCI method. However, states involving the $O1s^{-1}5\sigma^{-1}$ configuration were not calculated in this case and the energy range of peak 4 is not included in the interpretation based on SDCI.

Because the results of the SDCI method, which is less expensive in terms of CPU time compared to the CASPT2 method and hence more pragmatic, appear to fit best the experimental results, most of the peak assignments summarised in Table 5.1 are based on that method.

5.1.6 Auger decay of core-valence states

A core-valence doubly ionised state, similar to a single core hole, may decay by an Auger process. In Paper I this phenomenon has been studied by selecting three electron coincidence events, where two electrons are attributed to different peaks in the core-valence double ionisation spectra displayed in Figures 5.7 and 5.8, while the remaining electron constitute the Auger spectrum associated with the selected peak. Since the final states are triply ionised, the triple valence ionisation spectrum is also included for comparison.

As can be seen from Figure 5.9, the spectra associated with the $1s^{-1}v^{-1}$ vacancy of the same element are very similar in profiles, but shifted relative to each other. The shift approximately equals the energy differences between the corresponding peaks in the core-valence double ionisation spectra. The Auger spectra attributed to the decay of the formylic and methylic $C1s^{-1}$ holes do not reveal any significant differences between each other. The Auger spectra involving the $O1s^{-1}$ vacancy tend to populate higher tricationic states than the spectra involving one of the $C1s^{-1}$ vacancies, which perhaps is not unexpected since the Auger decays upon simple core hole formation shared already a similar difference. The onset of the Auger spectra is approximately the same as the onset of the triple valence ionisation spectrum, which supports the estimate of the lowest triple ionisation energy made in §5.1.6.

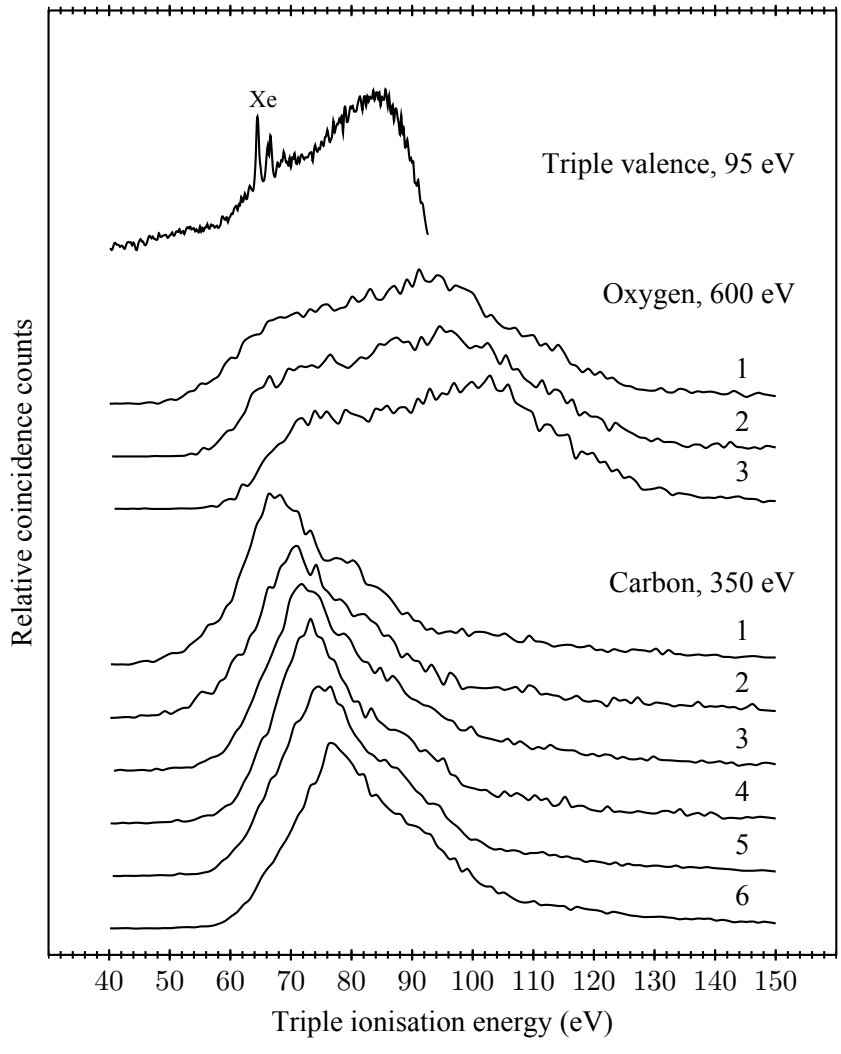

Figure 5.9. Auger spectra of core-valence states in acetaldehyde corresponding to the peaks with the same labels as used in Figures 5.7 and 5.8 in comparison with the triple valence ionisation spectrum. The photon energies are shown for each group of spectra.

5.1.7 Site-specific photodissociation

The electron-ion coincidence set-up described in §3.2.4 allows us to study photodissociation processes (§2.4) upon core ionisation of acetaldehyde on different molecular sites. Several previous investigations concentrated on element-specific [56–59] and site-specific [60–63] photodissociation of molecules upon core-excitation and subsequent resonant Auger decay. In contrast, fates of core-ionised states upon normal Auger decay are relatively little studied. Some previous works were devoted to the element-specific case [64–66] and only

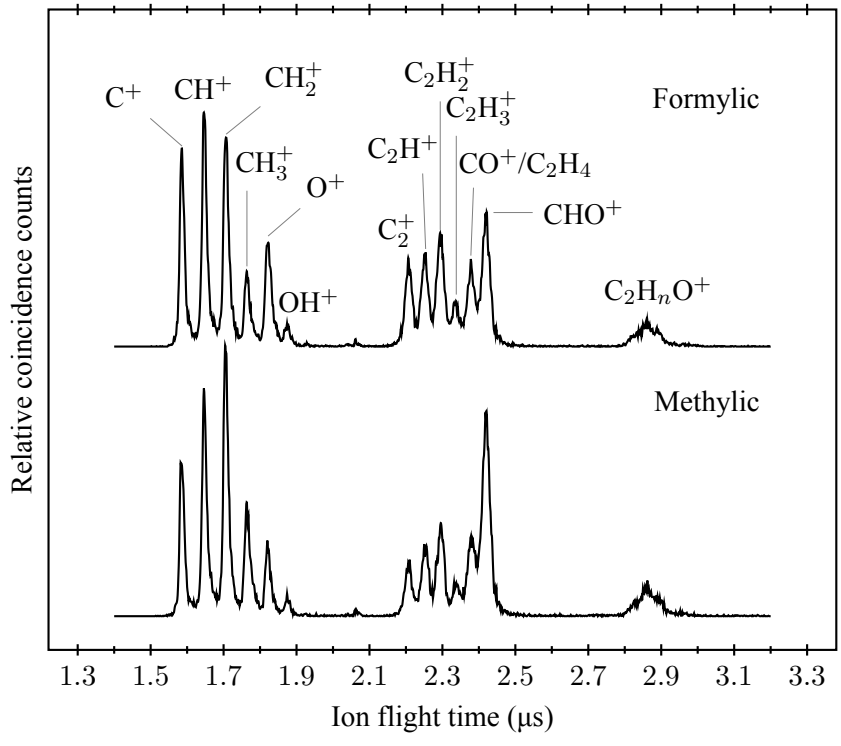

Figure 5.10. Mass spectra of acetaldehyde at the photon energy of 307 eV, measured in coincidence with either the formylic or methylic C1s photoelectron as labelled. Each spectrum is normalised to its total intensity. The bin size is 2 ns.

a few studies to site-specific dissociation of core-ionised molecules [67–71]. Recently, photodissociation of molecules upon core-ionisation of different carbon atoms were investigated by Itälä *et al.* [72] for pyrimidine and by Eland *et al.* [31] for ethyl trifluoroacetate. Paper III presents the study of site-specific photodissociation of acetaldehyde upon initial core photoionisation on either the formylic or methylic C1s level.

Figure 5.10 shows the mass spectra of fragments originating from core-ionised acetaldehyde as derived from coincidences between one ion and one C1s electron. The photon energy was 307 eV. The assignment of the spectra, which is also shown in Figure 5.10, is quite straightforward, taking into account that in acetaldehyde there are three atoms of relatively heavy elements of oxygen and carbon. In these spectra there are three groups of peaks corresponding to the different number of atoms of these elements: one for the faster group, two for the middle group and three for the slower one. The expected hydrogen ions H^+, H_2^+ and H_3^+ [73] are not detected, probably because their flight times are shorter than the ion detection delay, which was adjusted in order to avoid an influence from the ion extraction pulse on the electron sig-

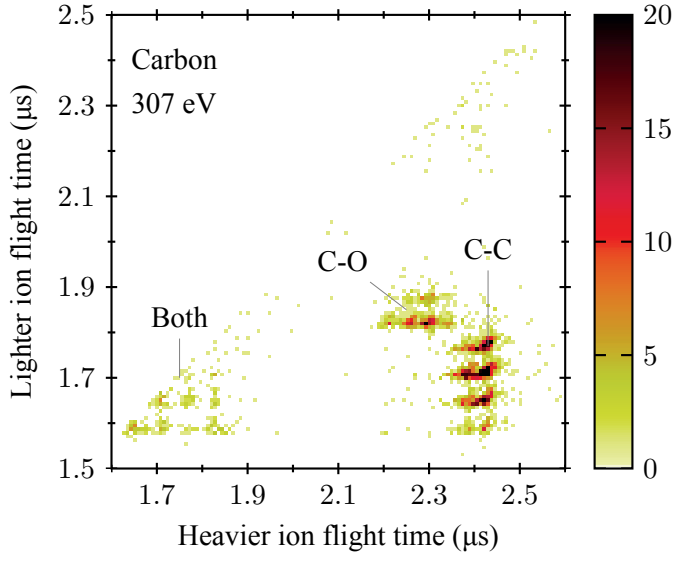

Figure 5.11. Acetaldehyde ion-ion coincidence map at the photon energy of 307 eV selected by any of the two C1s photoelectrons. The colour scale represents the coincidence counts within a particular bin. The events with an ion flight time difference < 40 ns are discarded. Bin size is 8 ns.

nal. The differences between the spectra are visible at once, but since single ions do not unambiguously reveal the associated fragmentation patterns, it is difficult to judge from these spectra on whether or not the process is truly site-specific, i.e. the bond breaks preferentially near the initial charge localisation. A thorough comparison for each mass peak was done in Paper III.

In order to investigate which fragmentation patterns are more likely to occur upon the ionisation on one or another C1s orbital, one can make use of three-fold coincidences between two ions and one core electron and represent the ions as an ion-ion coincidence map, where spots will represent the associated fragmentation patterns more unambiguously, than the peaks in a mass spectrum. An example of such a map is shown in Figure 5.11. Since the colour differences between maps selected separately by the methylic and formylic $C1s^{-1}$ lines are not pronounced enough to be visible in colour, the selection has been made here based on both lines, i.e. the map in Figure 5.11 reflects the superposition of processes associated with both sites. The spots on the map are divided into three groups. The bottom-left group consist of product pairs, where both have exactly one relatively heavy atom. This is possible only upon the dissociation of both the C-O and C-C bonds, thus it is labelled "Both". Due to the limited ability to detect particles arriving close in time, such as those with equal masses, for instance $CH^+ + CH^+$, not all possible events, which belong to this group are detected. This leads to an underestimated intensity of this group. The next group closest to the centre of the map consist of CH_n

($n = 0, 1, 2, 3$) products coincident with either O^+ or OH^+ and therefore implies the rupture of the C-O bond, which is used to the label this group. Finally, the group in the bottom-right corner of the map includes correlations between CO^+ or CHO^+ on the horizontal axis and CH_n ($n = 0, 1, 2, 3$) on the vertical one, which corresponds to the C-C bond breakage and is labelled accordingly.

Two maps similar to 5.11 have also been derived site-specifically by selecting in coincidence either the formylic or methylic C1s electron. The intensities of the different groups in percentage of the total area of each map are shown in Table 5.2. It demonstrates the site-specific nature of the dissociation process following the $C1s^{-1}$ photoionisation of acetaldehyde.

In general, the site-specific bond rupture, found above, can be thought to arise at least in two different ways. One of them is associated with differences in the population of the dicationic states upon normal Auger decay, which precedes the dissociation of the molecule. In Figure 5.3 we have already seen, that this population is quite different in the case of acetaldehyde. However, in principle, the fragmentation patterns can be different even if the Auger spectra would be exactly the same. In this alternative mechanism the individual dicationic states dissociate differently depending on the initial charge localisation. This is assumed to be possible because of the influence of the core hole on the nuclear motion within its few femtosecond lifetime, which in turn affects the fragmentation patterns of the individual dicationic states.

In order to find out how these two mechanisms may contribute to the site-specific difference, one should exclude the influence of different dicationic state population by selecting particular states and looking at their fate upon the formation of one or another $C1s^{-1}$ hole. Ideally this should be done using fourfold coincidence events, each of them consisting of two ions and both the core and Auger electron, but the statistics of the present data was not sufficiently high to allow this. Instead, threefold coincidence events comprising one ion and two electrons have been used here. This means, that instead of ion-ion coincidence maps, differences between mass spectra have to be analysed. Another issue is the high density of states in the Auger spectra of acetaldehyde, which makes it very difficult, if not impossible, to select a single individual dicationic state in practice.

Table 5.2. *Intensities of groups of spots corresponding to different bond rupture as shown in Figure 5.11 in percentage of the total area of a particular spectrum for the acetaldehyde ion-ion coincidence maps selected on either the formylic or methylic C1s photoelectron.*

Bond rupture	Formylic	Methylic
C-C	57.1 ± 2.6	68.1 ± 2.9
C-O	26.0 ± 1.5	20.0 ± 1.3
Both	16.9 ± 1.2	11.9 ± 1.0

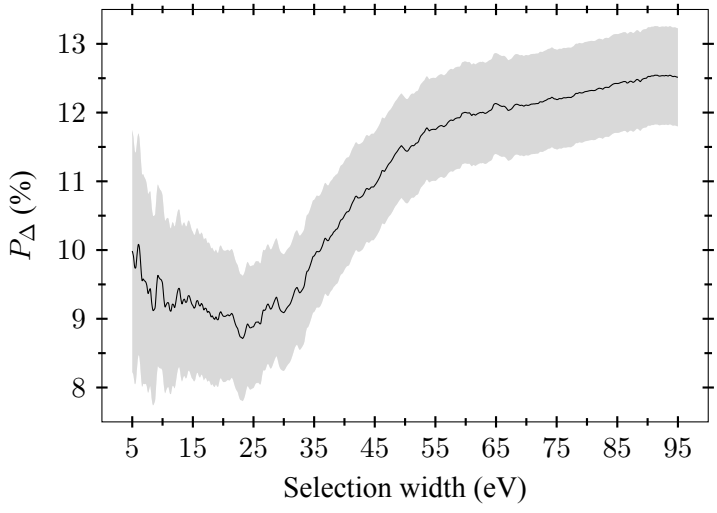

Figure 5.12. The total site-specific difference derived using Equation (5.1) between the integral intensities of the peaks in the mass spectra of acetaldehyde measured in coincidence with the formylic and methylic C1s electron and an Auger electron at the photon energy of 307 eV as a function of the double ionisation energy selection width. The centre of the selection is chosen near the maximum of the Auger spectra, i.e. at the double ionisation energy of 44 eV. The grey area represents the statistical uncertainty.

In Paper III a site-specificity parameter P_Δ was introduced in order to characterise site-specific differences between a pair of mass spectra, in this case associated with the initial removal of the formylic or methylic C1s electron. Prior to the parameter calculation, each spectrum has to be normalised to its total intensity and the background between the peaks has to be excluded. Then, the intensity of each peak has to be obtained by integrating over the peak width. The sum of all peak intensities in one mass spectrum is then equal unity. The parameter P_Δ is then defined as

$$P_\Delta = \frac{1}{2}\sum_{i=1}^{N} |p_{\mathrm{fi}} - p_{\mathrm{mi}}| \tag{5.1}$$

where p_{fi} and p_{mi} are the intensities of the i$^{\mathrm{th}}$ peak in the formylic and methylic spectra, respectively and N is the total number of peaks. P_Δ equals zero would mean exactly the same intensities of all peaks, i.e. no site-specificity, while P_Δ equals unity means that the spectra are totally different, i.e. have no common peaks. For convenience, in what follows we will express the results in terms of percentage.

The centre of the double ionisation energy selection range can be set at the maximum of the Auger spectra, which is found at about the same position in both the formylic and methylic case. Varying the width of this selection we can

include the dissociation of more or fewer dicationic states for the extraction of the mass spectra. Then P_Δ can be plotted as a function of the width of this selection, which is presented in Figure 5.12.

As can be seen, there is a plateau discernible at larger widths, which corresponds to the selection of the whole Auger spectrum range and therefore characterises the difference between the spectra in Figure 5.10, where the selection has been done only by core, but not Auger electrons. Towards narrower widths, the site-specificity decreases, reflecting a smaller contribution from the difference between the Auger spectra. However, for selection widths below 30 eV, another plateau is found. Though smaller widths below about 5 eV do not provide enough statistics, an extrapolation of the plateau suggests, that for selection widths approaching 0 eV, the site-specific difference seems to remain above 8%. From this we can conclude that both suggested mechanisms play roles in the site-specific photodissociation of acetaldehyde with more significant contributions from the differences in decay of the individual dicationic states due to nuclear motion within the lifetime of the core hole.

5.2 Carbon dioxide

Carbon dioxide is a centrosymmetric linear molecule with one carbon atom in between two oxygen atoms. There are many previous studies of its photodissociation including the involvement of highly charge states [74–79]. In a relatively recent study by Laksman *et al.* [80] it was found that O_2^+ is produced upon resonant C1s $\rightarrow \pi^*$ excitation at 290.7 eV. The study suggests, that this molecular rearrangement may occur by bending of the parent molecule. Another assumption of that work was that O_2^+ is formed mainly or even only from doubly ionised states created after double Auger decay because in Laksman's experiment O_2^+ was detected in coincidence with C^+. Paper IV examines both of these hypotheses using the electron-ion coincidence set-up described in §3.2.4.

Figure 5.13 shows mass spectra of core-excited carbon dioxide recorded at the photon energy of 290.7 eV, where ionic products are detected in coincidence with either one or two electrons, corresponding to single or double resonant Auger decays, respectively, and which are labelled accordingly. One can see from the figure, that the peak for O_2^+ is considerably more pronounced in single than in double ionisation, which rules out the second hypothesis by Laksman *et al.*. The double peak for O_2^+ in the double Auger decay case suggests, that the initial kinetic energy of O_2^+ is relatively high and the ions, emitted perpendicular to the flight tube axis, are not detected. In the single Auger decay case the width of O_2^+ peak is the same, but the central part is maintained, meaning that there are lower kinetic energy O_2^+ species in addition to the high energy product.

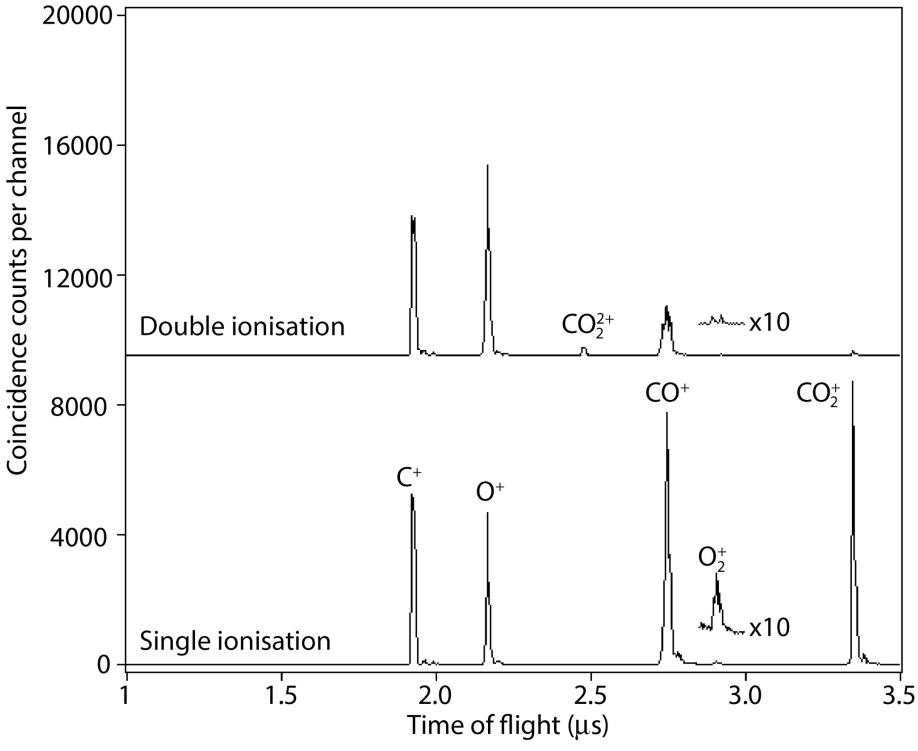

Figure 5.13. Mass spectra of carbon dioxide upon C1s $\rightarrow \pi^*$ excitation at the photon energy of 290.7 eV, measured in coincidence with either one or two Auger electrons labelled as "Single ionisation" or "Double ionisation", respectively.

Figure 5.14 also represents the mass spectra for different ionisation stages of carbon dioxide, but for the data taken at the photon energy of 350 eV, which is above the C1s ionisation threshold, i.e. the C1s electron can be completely removed to the continuum. The spectra associated with double and triple ionisation are derived from coincidence events with one ion and either two or three electrons, respectively, where the energy of one of the electrons is selected to lie within the range of the C1s line. Therefore, they correspond to double and single $C1s^{-1}$ Auger decay, similarly to the spectra in Figure 5.13, but upon core ionisation rather than excitation. The single ionisation spectrum is taken in coincidence with one valence electron. In contrast to the resonant case, neither double nor single normal Auger decay leads to the formation of O_2^+. Also, it can be noted, that C^{2+} is formed only in the case of triple ionisation by double Auger decay, but not in the two other cases.

The period of vibrations in carbon dioxide is about 50 fs, while the lifetimes of the core holes are about 6 fs for $C1s^{-1}$ and about 3.5 fs for $O1s^{-1}$, which means that the bending is not possible during the presence of the core vacancy and it is therefore necessary for the formation of O_2^+ that the molecule is bent already when the photon gets absorbed as proposed by Laksman *et al.* [80].

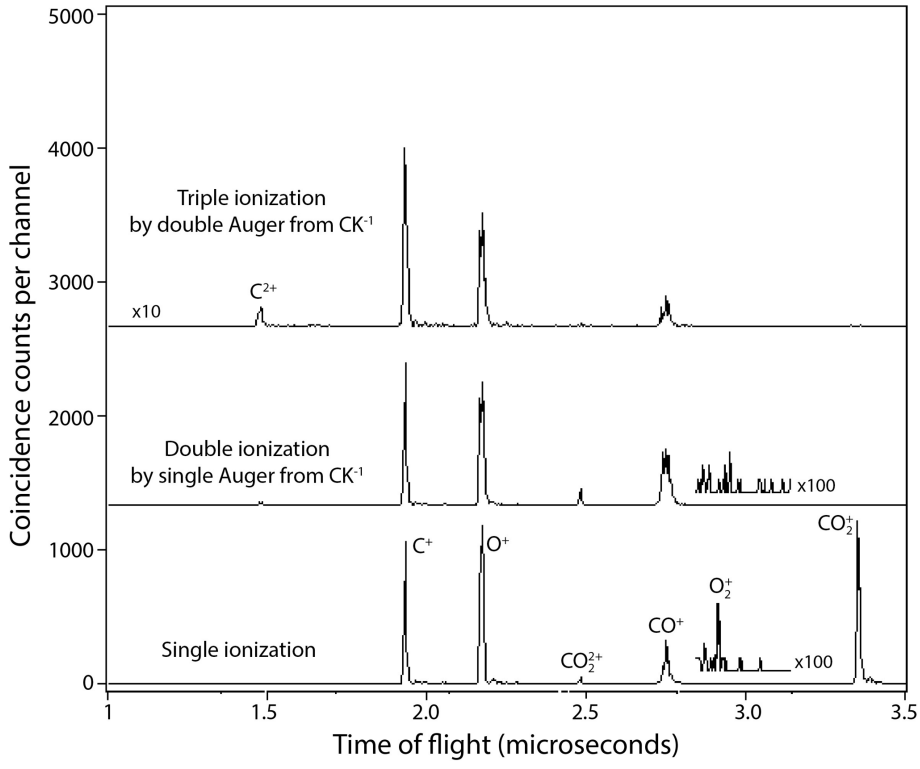

Figure 5.14. Mass spectra of carbon dioxide at the photon energy of 350 eV, measured in coincidence with one, two or three electrons as labelled. In the cases of double and triple ionisation, one electron has been selected to correspond to the C1s photoelectron line.

Since the lifetimes of core-ionised and core-excited states are similar, this condition has probably no effect on the differences in formation of O_2^+. Instead, the bonding character of the π^* orbital could play a role. Shake-up processes to the π^* orbital could also be a reason for the presence of O_2^+ in coincidence with valence ionisation.

5.3 Xenon

Being one of few atomic species easily available in gas bottles from the shelf, Xenon is a well-studied sample both experimentally [81–83] and theoretically [84]. However, most of the studies on the decay of inner shell holes concentrated so far mainly on the $4d^{-1}$ and $4p^{-1}$ holes while leaving deeper core holes relatively unexplored. In this study the electron-ion coincidence set-up with the newly developed perpendicular mounting of the ion detector with respect to the electron flight tube described in §3.2.5 has been used, which allowed us to select almost pure charge states. This is an advantage in comparison to most of

Table 5.3. *Branching of different inner shell holes in Xenon in percentage.*

	$4d_{5/2}$	$4d_{3/2}$	'4p'	4s	3d	$3p_{3/2}$	$3p_{1/2}$
Xe^{2+}	83.7±1	79.5±1	3±1.5				
Xe^{3+}	16.3±1	20.5±1	62±3	34±10	4.7±0.2		
Xe^{4+}			35±7	35±8	53.7±1	3±0.8	3.2±1.5
Xe^{5+}				30±5	25.6±1	16.8±0.8	9.1±2.2
Xe^{6+}					13±0.5	28.3±2	27.2±3.3
Xe^{7+}					2.4±0.3	38.6±3.6	39.6±3.6
Xe^{8+}					0.4±0.2	11.5±1.5	16.4±2.4
Xe^{9+}						1.7±0.6	4.5±1

previously used methods, which were not able to exclude the resonance states below and shake-up states above the ionisation thresholds. The investigation presented in Paper V has determined branching ratios to final Xen^+ states with $2 < n < 9$ from pure $4d^{-1}$, $4p^{-1}$, $4s^{-1}$, $3d^{-1}$ and $3p^{-1}$ Xe^+ hole states, with resolution of the spin-orbit substates.

Table 5.3 gives the resulting branching ratios. As can be seen, deep inner shell holes mostly populate higher charged states. These results have been compared with theoretical predictions by Kochur *et al.* [84], which turned out to be accurate for all but the highest charges. A severe underestimation of the highest charges is the case for all calculations. This is likely due to exclusion of electron correlations, which must be playing a significant role in the decay as shown by Penent *et al.* [35] for the case of the Xenon 4d hole. For the deeper inner shell holes, where Coster-Kronig transitions are dominant, coherent two-electron decay is less significant, but still contributes particularly to formation of the most highly charged ions.

As a final remark, the results for the 3d and 3p core hole states are, to the best of our knowledge, the most comprehensive and reliable data available at the moment.

6. Summary and Outlook

In this thesis, multiple ionisation processes of acetaldehyde, carbon dioxide and Xenon, initiated by single photon absorption, were investigated by means of a state-of-the-art multi-electron-ion coincidence spectroscopy method based on the time-of-flight magnetic bottle technique. Primarily, the synchrotron radiation facility BESSY II at the Helmholtz Zentrum in Berlin was employed as the ionisation source, which enabled access to not only valence, but also core levels, revealing several different processes promoting the target systems into different charged states.

A particular focus of this thesis work was on double and triple ionisation processes of acetaldehyde in the valence region as well as on single and double normal Auger decay of initial 1s core vacancies. The double valence ionisation electron spectrum of acetaldehyde was found to be very similar to the known $O1s^{-1}$ Auger spectrum of this species [47] which was used as the basis for the assignment of the spectral features observed. With the coincidence technique at hand, single Auger decay spectra could be extracted site-selectively for the case of the two chemically different carbon 1s core holes of acetaldehyde. The spectra associated with the formation of the formylic and methylic core vacancies were found to be substantially different from each other, and are in good agreement with theoretical predictions from 1995 [49]. A similar distinction was found for the double Auger spectra of acetaldehyde for which no theoretical predictions exist so far. Also, Auger decay spectra of shake-up satellite states of acetaldehyde were revealed for the first time and showed that the spectator process is dominant.

In a related study of acetaldehyde double ionisation spectra involving the simultaneous emission of a core and a valence electron were investigated in the light of a previously established empirical model. Because this model could not explain satisfactorily all the gross features observed, the core-valence spectra of acetaldehyde were used as a testbed for analysing this kind of spectra by means of quantum chemical electronic structure methods of increasing sophistication. While the two simplest models, based on interaction corrected Hartree-Fock orbital energies or the Z+1 approximation, were found to provide a fast orbital interpretation of core-valence spectra, in particular in the low energy parts, the interpretation of the full spectra require primarily correlated models, of which the CASPT2 method is, without any doubt, the most sophisticated, but also most expensive in terms of the CPU time required. A more pragmatic way suggests SDCI calculations, which use Hartree-Fock orbitals for the ground state and core-relaxed orbitals for the core-valence ionised

states, thereby combining several aspects that are important for modelling this kind of states. Further investigations of core-valence states of different systems is needed in order to understand in which cases the empirical model is applicable and to explore more the applicability of different quantum chemical methods.

In investigating mass spectra of acetaldehyde in coincidence with the electrons emitted at a photon energy above the two chemically different carbon 1s core levels, site-specific effects of the initial charge location were uncovered. Breakage of the C-C bond appears to be more probable while breakage of the C-O bond is less probable after core ionisation at the methylic carbon atom rather than the formylic carbon atom. Furthermore, breakage of both the C-C and C-O bonds is more likely after formylic carbon ionisation. Possible mechanisms giving rise to such site-specific effects were discussed, and with the aid of a site-specificity parameter P_{Δ} originally defined in this work it is suggested that differences in fragmentation behaviour between initial ionisations at the formylic and methylic carbon atoms probably persist even for identical internal energy contents in the nascent dications. The applicability of P_{Δ} is not limited only to the site-specific differences in photodissociation of acetaldehyde, but it can quantitatively characterise differences between any given pair of mass spectra. It can also be generalised for multi-dimensional ion data, characterising the differences in full fragmentation patterns.

Other multi-coincidence experiments with detection of both electrons and ions focused on the decay of core-excited and core-ionised states of carbon dioxide and confirmed previous investigations that the product O_2^+ is formed specifically in Auger decay from the C1s $\rightarrow \pi^*$ and O1s $\rightarrow \pi^*$ resonances. This led to the conclusion, that the molecular rearrangement necessary for the formation of the O_2^+ species is driven by the presence of an electron in the π^* orbital. In addition, this work revealed that O_2^+ is produced by both single and double Auger decay.

Finally, within the framework of this thesis work a new variant of the multi-electron-ion coincidence method involving a magnetic bottle, has been devised, where the ion time-of-flight spectrometer is mounted perpendicularly to the electron flight tube. In this way, the electron resolution, which was compromised in the original multi-electron-ion in-line set-up used before, is essentially preserved. Furthermore, this new set-up allows for position sensitive detection of the ions. In a first experiment making use of tunable soft X-rays, the branching ratios to final Xe^{n+} states with $2 < n < 9$ from the $4d^{-1}$, $4p^{-1}$, $4s^{-1}$, $3d^{-1}$ and $3p^{-1}$ Xe^+ hole states were investigated. These branching patterns can be regarded as a prototype for the creation of highly charged molecules by inner shell ionisation of substituent heavy atoms such as iodine. Of course, in molecules, an additional step, possible at all stages of the Auger cascades, will be intra-molecular charge transfer, which typically occurs on the femtosecond time scale. To this end, timing experiments with femtosecond resolution will be needed to characterise the charge evolu-

tion in detail and its likely competition with nuclear motion. By selecting the ejected electrons by number and energy, as done in Paper V, one can potentially select single charge states; the ability to do this for molecular ionisation is foreseen to be a great asset in forthcoming systematic studies of the dynamics of Coulomb explosions. Understanding these explosions is vital for the "diffract before destroy" structure determination technique at X-ray Free Electron Lasers (X-FELs) [85], where they are recognised as limiting factors. This constitutes currently one of the hot topics investigated at Free Electron Laser sources [86, 87].

7. Popularvetenskaplig sammanfattning på svenska (Popular science summary in Swedish)

Studier av enkel-foton multipel-jonisationsprocesser av atomer och molekyler med hjälp av koinsidensspektroskopi.

Viktig kunskap om materien i universum (av vilken 99% är joniserad) och på jorden erhålls genom spektroskopi, som bygger på växelverkan mellan ljus och materia. Sedan mer än 100 år tillbaka är spektroskopi ett enastående framgångsrikt forskningsfält i Sverige representerat av internationellt kända forskare som Anders Jonas Ångström, Johannes Rydberg, Manne Siegbahn och Kai Siegbahn, som inspirerar många av dagens forskare till en fortgående utveckling av nya metoder och mätteknologier vid avancerade ljuskällor. Min avhandling bygger på att med nya mätmetoder grundade på korrelationsspektroskopi och moderna ljuskällor som synkrotronljusanläggningar studera dynamiska processer och struktur vid två- eller flerfaldig jonisering av materien.

Om en neutral atom, en materiens byggsten bestående av elektroner som omger en kärna innehållande protoner och neutroner, utsätts för strålning t.ex. solljus, och om strålningen innehåller ljuspartiklar (dvs. ”fotoner”) med tillräcklig hög energi, dvs. energi inom de så kallade vakuum-ultravioletta eller mjukröntgenområdena, kan elektroner frigöras från den. Detta fenomen förklarade Albert Einstein år 1905 med den fotoelektriska lagen.

Två eller fler atomer kan kombinera till en ny enhet kallad molekyl (eller till kondenserat ämne) genom att de delar på elektronerna. Det är en mycket väsentlig aspekt för på detta sätt uppstår de kemiska bindningar som håller samman materien.

När en elektron, som bär den minsta möjliga negativa laddningen, avlägsnas från en neutral atom eller molekyl, skapas ett positivt laddad system, dvs. en jon. Den avlägsnade elektronen har enligt fotoelektriska lagen en väl definierad rörelseenergi, och bär därför med sig information om vad som händer inne i atomen eller molekylen.

I mitten av 1950-talet utvecklades av bl.a. prof. Kai Siegbahn och hans medarbetare i Uppsala en metod för att mäta ”fotoelektroners” rörelseenergi, kallad fotoelektronspektroskopi. Denna metod visades av forskarna i Uppsala på ett tidigt stadium vara ytterst känslig för den kemiska sammansättningen av materien (på engelska: Electron Spectroscopy for Chemical Analysis (ESCA)) eftersom bindningsenergin för i synnerhet de starkast bundna elektronerna (de som befinner sig närmast kärnan) visar sig vara karakteristisk för vart och ett

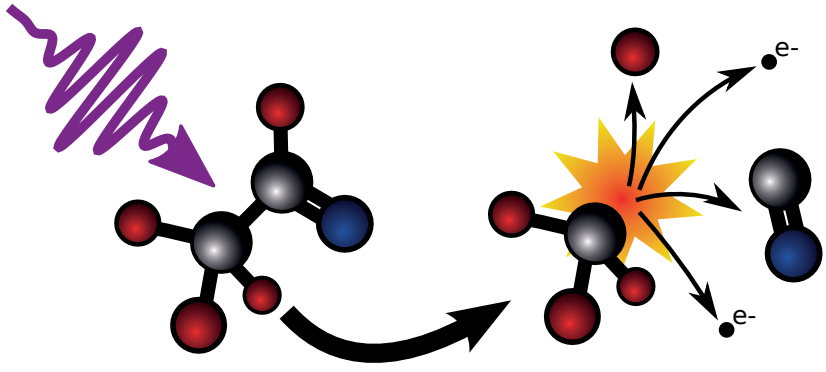

Figur 7.1. Illustration av multipel jonisation av acetaldehyd orsakad av en infallande foton.

av grundelementen, dvs. för atomerna som vi känner till från Mendelejevs periodiska system.

Om fler elektroner frigörs samtidigt från en atom (molekyl) under inverkan av en foton, så är det mycket viktigt att kunna analysera alla dessa tillsammans, eftersom de är korrelerade till varandra, och var och en för sig bär viktig delinformation om systemet. Sådana experiment kräver s.k. korrelationsmetoder.

En nära samarbetspartner, prof. John Eland vid universitet i Oxford, är känd världen över för hans utveckling av mycket effektiva mätmetoder för korrelationsspektroskopi, bl.a. PIPICO (som står för ”PhotoIon-PhotoIon Coincidence”) eller PEPICO (som står för ”PhotoElectron PhotoIon Coincidence”). För några år sedan presenterande han en, fram till idag, världsledande korrelationsteknik för energianalys av två eller flera elektroner från en och samma atom (molekyl), ”samtidigt”. Metoden heter ”Time-Of-Flight PhotoElectron-PhotoElectron COincidence (TOF-PEPECO) spectroscopy”. Den bygger på mätning av de frigjorda elektronernas ”flygtid” i ett några meter långt rör, och eftersom man känner rörets längd är det lätt att ur flygtiden räkna ut elektronernas rörelseenergi.

Eftersom elektronerna ansvarar för bindningarna i molekyler, kan en molekyl falla isär, dvs. dissociera, om man avlägsnar elektroner, som den schematiska bilden, Figur 7.1, illustrerar. Detta kan leda till fler laddade fragment (joner), och för att kunna få en helhetsbild krävs det att jonerna analyseras tillsammans med elektronerna. Under en längre forskningsvistelse i prof. Elands grupp blev min huvudhandledare, prof. Raimund Feifel, involverad i en första vidareutveckling av TOF-PEPECO-tekniken med tillägg av en jon-detektor, som ledde till registrering av de första ”Time-Of-Flight PhotoElectron-PhotoElectron PhotoIon-PhotoIon Coincidence (TOF-PEPEPIPICO)” data någonsin.

Efter prof. Feifels hemkomst från Oxford byggde han upp en forskningsverksamhet kring multi-elektron-jon-korrelationsspektroskopin där bland annat två världsledande TOF-PEPE(PIPI)CO-instrument, som överfördes i sam-

band med prof. Elands pensionering, ingår. Ett av dessa forskningsinstrument har varit av avgörande betydelse för mitt avhandlingsarbete, som baseras på användning av TOF-PEPE(PIPICO)-tekniken för multi-elektron-jon-koincidensstudier av atomer och molekyler. På senare tid har vi genom vidareutveckling av jondetektionsdelen även lyckats erhålla positionskänslig information som avslöjar bl.a. vinkelberoende i emissionen av jonerna samt deras relaterade rörelsemängdsmoment.

Mitt avhandlingsarbete koncentreras främst på studier av multi-elektronemissionsprocesser i acetaldehyd, CH_3CHO, som är en intressant molekyl eftersom den innehåller två kolatomer som är omgivna av andra, kvalitativt olika grundämnen, en syreatom och flera väteatomer. Detta ger upphov till en väsentlig skillnad i bindningsenergi (2.65 eV) för de innersta elektronerna hos de två kolatomerna som i litteraturen kallas för ”chemical shift”.

Framstegen gällande acetaldehyd, som gjorts inom ramen för min avhandling, är mångfaldiga och gäller t.ex. karakterisering av dess elektronstruktur och efterföljande dissociationsprocesser när två eller fler elektroner frigörs. Jag har fokuserat bl.a. på hur två eller tre elektroner, som lämnar en acetaldehydmolekyl, delar på den av systemet absorberade fotonenergin och vilka sluttillstånd som skapas. Genom att variera fotonenergin kunde vi på ett kontrollerat sätt frigöra antingen främst elektroner som normalt befinner sig långt bort från kärnan (s.k. valenselektroner) eller en kombination av elektroner, som befinner sig nära kärnan (s.k. innerskalselektroner), samt valenselektroner. Emissionen kan ske i form av en direkt, dvs. simultan, jonisationsprocess eller i form av sekventiella processer där först innerskalselektronen avlägsnas i en primär process och sedan en eller flera valenselektroner utsänds i sekundära processer. Det senare förloppet är också känt i litteraturen som Augersönderfall. Det väsentligt nya i min avhandling är att vi med hjälp av TOF-PEPECO-tekniken har kunnat studera bland annat dessa Augersönderfall specifikt för två kvalitativt olika kolatomer i acetaldehyd. Delvis har studierna gjorts i direkt jämförelse med teoretiska förutsägelser från tidigt 90-talet som inte tidigare har kunnat undersökas experimentellt på ett vederhäftigt sätt på grund av avsaknad av lämplig mätteknik.

I nära samarbete med våra teoretiska kollegor på KTH i Stockholm och på Oulu universitet har vi nu undersökt systematiskt hur man på ett säkert sätt kan förklara så kallade innerskals-valens (på engelska: ”core-valence”) - dubbeljonisationsspektra av acetaldehyd. I studierna utgick vi från en empirisk modell som presenterades i tidigare arbeten, samt använde vi oss av successivt alltmer avancerade kvantkemiska beräkningsmetoder.

En annan ny aspekt på acetaldehyd som jag har undersökt inom ramen för min avhandling rör dissociationsprocessens beroende av från vilken kolatom innerskalselektronen kommer. Genom att detektera både de elektroner och de joner som skapas i enskilda fotojonisationsprocesser kunde vi påvisa stora skillnader i fragmenteringseffekter för de två kolatomerna.

Inom ramen för min avhandling genomförde vi även en liknande fragmenteringsstudie av koldioxid samt presenterade de första multi-elektron-jon koincidensdata som vi åstadkom med den senaste varianten av TOF-PEPEPIPICO-tekniken. I den senare studien fokuserade vi på populationen av diverse jonladdningstillstånd i xenon som en funktion av innerskalsvakansen.

Resultaten som presenteras i min avhandling förväntas bli vägledande för den fortsatta utvecklingen av området, som redan har börjat t.ex. vid fria-elektron-laser-anläggningarna LCLS på Stanford, FERMI i Trieste och FLASH i Hamburg. Vår egen forskargrupp avser i denna utveckling att använda sig av TOF-PEPEPIPICO-tekniken anpassad på lämpligt sätt till dessa anläggningar.

8. Краткое научно-популярное изложение на русском (Popular science summary in Russian)

Исследование однофотонной многократной фотоионизации атомов и молекул при помощи спектроскопии совпадений: позиционно-специфичные эффекты в ацетальдегиде и углекислом газе.

Данная работа посвящена изучению свойств атомов и молекул — мельчайших частиц вещества, из которых состоит всё, что нас окружает, как и мы сами. Атомы состоят из положительно заряженного ядра и электронов. Количество электронов в нейтральном атоме равно зарядовому числу ядра, таким образом положительный и отрицательный заряды друг друга компенсируют. Зарядовое число ядра определяет химический элемент данного атом. Например, 1 — это водород, 2 — гелий, 12 — углерод, 16 — кислород, а 54 — ксенон. Электроны в атоме располагаются на орбиталях, причём не более двух электронов на одну орбиталь. Орбитали распределены по оболочкам. На первой оболочке только одна орбиталь (она обозначается 1s), на второй — четыре, на третьей — девять и так далее. Количество занятых электронами оболочек, для нейтрального невозбужденного атома соответствует номеру строки в таблице Менделеева для данного элемента. Оболочки с меньшим номером называются внутренними, а с бóльшим — внешними.

Несколько атомов могут объединиться в молекулу, образовав химическую связь. В этом случае электроны, в основном с внешних оболочек, образуют новые, молекулярные, орбитали, которые становятся делокализованными, то есть принадлежат не конкретному атому, а всей молекуле. Такие электроны, а так же орбитали и оболочки, в которых они распложены, называют валентными. Электроны с внутренних оболочек, которые практически не принимают участие в связи и остаются локазованными, называются остовными.

Одной из важнейший характеристик орбитали является энергия ионизации — энергия, которую необходимо затратить, чтобы удалить из атома электрон, находящийся на данной орбитали. Для орбиталей внутренних оболочек эта энергия больше, то есть их электроны связаны с ядром сильнее, чем электроны внешних оболочек. А для одной и той же орбитали энергия ионизации больше у элементов с бóльшим зарядовым числом. Например, в Таблице 3.1 (стр. 19) показаны значения (в электронвольтах,

эВ) энергии ионизации 1s электронов для элементов второй строки таблицы Менделеева.

Атомы и молекулы, в которых недостаточно электронов, чтобы скомпенсировать положительный заряд ядра или ядер называются положительными ионами. В таких ионах из-за доминирования положительного заряда электроны связаны сильнее, чем в нейтральном атоме или молекуле. Таким образом, энергия двукратной ионизации выше, чем сумма двух энергий однократной ионизации для той же пары орбиталей. Таким образом, электронная структура ионов отличается от таковой у нейтральных атомов и молекул и требует отдельного изучения посредством многократной ионизации.

Явление, которое изучается в данной работе называется фотоионизация, открытая Генрихом Герцем в 1887 году. и объяснённая Альбертом Эйнштейном в 1905 году. Суть явления состоит в испускании электронов атомами или молекулами при поглощении фотона. Фотон — это мельчайшая частица электромагнитного излучения, в частности света. Свет имеет энергию фотона в диапазоне от 1.6 эВ (красный) до 3.2 эВ (фиолетовый). Такой энергии достаточно для возбуждения атомов или молекул, то есть для переноса электронов на незанятые орбитали, слабее связанные с ядром, но недостаточно для ионизации атомов одним фотоном. Поэтому мы используем фотоны более высоких энергий, соответствующие вакуумному ультрафиолету, а так же рентгеновскому излучению.

Для извлечения электронов валентных оболочек необходимы десятки эВ, тогда как в случае остовных орбиталей требуются сотни или даже тысячи эВ. Для генерации рентгеновских фотонов с минимальным разбросом по энергиям вокруг заданного значения используются синхротронные источники, такие как BESSY II в Берлине, который использовался для большинства экспериментов в рамках данной работы.

Многократная фотоионизация может происходить различным образом. Один из возможных путей — это нормальный эффект Оже, проиллюстрированный на Рисунке 2.1(a) (стр. 15). В простейшем случае это двуступенчатый процесс, где на первом этапе выбивается остовный электрон, образуя так называемую остовную дырку, которая через несколько фемтосекунд (10^{-15} сек.) заполняется электроном из внешней оболочки. Высвобождаемая при этом энергия может передаться третьему электрону, который так же покидает молекулу, в этом случае называясь Оже электроном в отличие от фотоэлектрона, испущенного на первом этапе. Конечным состоянием такого процесса является ион с двойным положительным зарядом. Оже-распад также может быть многократным, приводя к зарядовым состояниям бóльшей кратности. Кроме того, существует резонансный Оже-процесс, показанный на Рисунке 2.1(b,c), в котором на первом этапе остовный электрон не ионизуется, а возбуждается.

Многократная ионизация так же может произойти напрямую, то есть с одновременным выбиванием двух и более электронов без промежуточно-

го состояния, как показано на Рисунке 2.2 (стр. 16). В этом случае, энергия поглощённого фотона, превышающая энергию двукратной ионизации, распределяется между испущенными электронами случайным образом и преобразуется в энергию их поступательного движения (кинетическую энергию), что контрастирует с Оже-процессом, где распределение задаётся взаимными расположением вовлечённых в процесс орбиталей по шкале энергий.

Поскольку электроны находящиеся на связывающих валентных молекулярных орбиталях составляют химическую связь, их удаление в процессе фотоионизации может приводить к разрыву связи — явлению, называемому фотодиссоциацией. Достаточно сложные молекулы могут распадаться вероятностным образом по нескольким каналам. Так же при фотодиссоциации возможно образование новых связей между прежде не связанными напрямую атомами — молекулярная перегруппировка.

Экспериментальный техника для изучения фотоионизации с помощью измерения кинетических энергий испускаемых электронов называется фотоэлектронная спектроскопия, разработанная в 1960-х несколькими группами под руководством Девида Тёрнера [2] в Имерском колледже Лондона, Фёдора Ивановича Вилесова [3, 4] в Ленинградском Государственном Университете и Кая Сигбана здесь, в Уппсальском университете [5, 6]. Сигбан был удостоен Нобелевской премии за свой вклад в данную разработку. На данный момент это уже устоявшийся и широко применяемый метод характеристики электронной структуры атомов и молекул, а так же для определения неизвестного химического состава образца. Однако, традиционная фотоэлектронная спектроскопия неспособна соотнести детектированные электроны между собой, как относящиеся к одному событию ионизации в конкретной молекуле и, таким образом, она имеет очень ограниченные возможности по изучению корреляций между электронами, простейшим случаем которой является прямая многократная ионизация, описанная в предыдущем абзаце.

Времяпролётная спектроскопия совпадений на основе принципа магнитной бутылки [32], разработанная Джоном Иландом [7] в Оксфорде в 2003 году, является развитием техники фотоэлектронной спектроскопии, позволившим решить вышеобозначенную проблему. В нашем спектрометре, изображённом на Рисунке 3.3 (стр. 24), струя газа, выпущенная из полой иглы (обозначена как «Gas needle»), пересекается с импульсным электромагнитным излучением $h\nu$ в вакууме. Образовавшиеся электроны захватываются магнитным полем, образованным постоянным магнитом (обозначен как «Magnet») и соленоидом (обозначен как «Solenoid») и направляются в экранированную пролётную трубку с детектором на другом конце (обозначен как «MCP Detector»). Измеряется время пролёта электрона через трубку, откуда вычисляется его кинетическая энергия. Параметры эксперимента подбираются таким образом, чтобы частота импульсов была на порядок выше частоты событий ионизации. То есть

подавляющее большинство импульсов не вызывает ионизации образца. Таким образом, когда событие ионизации всё-таки происходит, вероятнее всего была ионизировна только одна молекула (атом) и все детектированные электроны относятся именно к этому событию.

Данный спектрометр также был модифицирован для одновременного детектирования как электронов, так и ионов, образовавшихся в процессе фотоионизации. Версия, разработанная Джоном Иландом и Раймундом Файфелем [8] показана на Рисунке 3.4 (стр. 3.4), где вместо конического магнита использован полый магнит, комбинированный с масс-спектрометром Уайли-Макларена [37]. В данной модификации ионы ускоряются киловольтным потенциалом в сторону, противоположную электронам, как только последние окажутся в пролётной трубке, дополнительно экранированной металлической сеткой.

В новой модификации, представленной в рамках этой работы, детектирование электронов и ионов происходит в перпендикулярном направлении, как показано на Рисунке 3.5 (стр. 3.5). Это позволяет не терять разрешение для энергий электронов из-за использования полого магнита в предыдущей модификации. Так же, новый масс-спектрометр оборудован позиционно-чувствительным детектором, который позволяет воспроизвести направления начальной скорости при образовании ионов.

Одним из образцов, исследованных в данной работе был ацетальдегид (этанал). Его структурная формула представлена на Рисунке 1.1 (стр. 11). Основной особенность его является наличие двух атомов углерода (символ C): один из них относится к альдегидной группе ($-CHO$), а другой — к метильной ($-CH3$). Из-за влияния окружения, энергии ионизации 1s уровня у них отличаются. С помощью спектроскопии совпадений можно изучать позиционно-специфичные эффекты, то есть различия в процессах ионизации, связанные с тем, какая C1s остовная дырка была создана при ионизации.

Для начала, были исследованы различные двух- и трёхэлектронные процессы в ацетальдегиде: прямая двукратная и трёхкратная ионизация, позиционно-специфичные одинарный и двойной Оже-процесс, а так же Оже-распады 1s дырок, возникших при одновременном возбуждении или ионизации валентного электрона.

Так же была исследована остовно-валентная двукратная фотоионизация ацетальдегида, при которой одновременно испускаются один остовный и один валентный электрон. Была опробована ранее предложенная эмпирическая модель для интерпретации остовно-валентного спектра, которая предполагает наложение сдвинутого спектра однократной валентной ионизации с установлением взаимно-однозначного соответствия пиков в двух спектрах. В этом случае пики остовно-валентного спектра интерпретируются как ассоциированные с ионизацией одного из электронов с той же валентной орбитали, что и соответствующие пики спектра однократной валентной ионизации, но в сочетании с остовным элек-

троном. Данная модель успешно дала интерпретацию низкоэнергетичной (по энергии ионизации) части остовно-валентного спектра ацетальдегида, включающего $C1s^{-1}$ вакансии, но оказалась совсем не способна описать остовно-валентный спектр, включающий $O1s^{-1}$ остовную дырку. Для полной интерпретации данных спектров коллаборирующей с нами теоретической группой была осуществлена серия квантово-химических вычислений.

Третье исследование посвящено фотодиссоциации ацетальдегида в зависимости от локализации изначальной остовной дырки на том или другом атоме углерода. Было показано, что вероятность разрыва связи, вблизи изначальной дырки выше, чем на отдалении, то есть при ионизации на альдегидном углероде увеличивается вероятность разрыва C-O связи, чем по сравнению с ионизацией на метильном углероде. А для ионизации на метильном углероде, наоборот, увеличивается вероятность разрыва C-C связи. Были рассмотрены два механизма для данного позиционно-специфичного эффекта и предложен способ определения количественного вклада каждого из механизмов, с помощью которой было установлено, что оба механизма играют заметную роль.

Ещё одно исследование касалось фотодиссоциации углекислого газа. Мы сравнили каналы диссоциации C1s дырки при нормальном и при резонансном Оже-распаде на π^* орбиталь. Было установлено, что молекулярная перегруппировка с образованием O_2^+ возможна только в резонансном процессе, что позволяет сделать вывод, что решающую роль в образовании данного продукта играет π^* орбиталь.

Наконец, с применением новой экспериментальной конфигурации, благодаря высокому разрешению давшей возможность делать выборку по чистым зарядовым состояниям, были измерены относительные вероятности различных зарядовых состояний при Оже-распаде остовных дырок на $4d^{-1}$, $4p^{-1}$, $4s^{-1}$, $3d^{-1}$ и $3p^{-1}$ орбиталях.

9 Acknowledgements

I have now filled so many pages with text and am pretty tired now after a period of hard work, that I shall keep this section short. I would very much like to thank following people for all their support during my Ph.D. studies: Raimund Feifel, Vitali Zhaunerchyk, Melanie Mucke, John Eland, Richard Squibb, Per Linusson, Håkan Rensmo, Olof Karis, Jan-Erik Rubensson, Hans Siegbahn, Svante Svensson, Leif Karlsson, Andreas Hult Roos, Jonas Andersson, Raj Singh, Vasyl Yatsyna, Omid Talaee, Dimitris Koulentianos, Craig Slater, Alexandra Lauer, Stacey Sörensen, Hans Ågren, Olav Vahtras, Kari Jänkälä and Matti Vappa.

Furthermore, I would like to acknowledge the Swedish Research Council (VR) and the Knut and Alice Wallenberg Foundation for the generous funding which they provided and without which my thesis work would not have been possible, as well as all Swedish tax payers for financial contribution to my salary.

Finally, I would like to thank both Uppsala University and the University of Gothenburg as my hosts.

References

[1] H. Ågren, A. Cesar, and C.-M. Liegener, "Theory of Molecular Auger Spectra," in *Advances in Quantum Chemistry* (P.-O. Löwdin, J. R. Sabin, and M. C. Zerner, eds.), vol. 23, pp. 1–82, Academic Press, 1992.

[2] D. W. Turner and M. I. Al Jobory, "Determination of Ionization Potentials by Photoelectron Energy Measurement," *The Journal of Chemical Physics*, vol. 37, no. 12, pp. 3007–3008, 1962.

[3] F. I. Vilesov, B. L. Kurbatov, and A. N. Terenin, "Energy distribution of electrons in photoionization of aromatic amines in gaseous phase," *Reports of The Academy of Sciences of the USSR*, vol. 138, pp. 1329–1332, Dec 1961.

[4] F. I. Vilesov, V. I. Kleimenov, and Y. V. Chizhov, "Photoelectron spectroscopy," *Advances in Photonics*, vol. 2, pp. 3–40, 1971.

[5] K. Siegbahn, C. Nordling, A. Fahlman, R. Nordberg, K. Hamrin, J. Hedman, G. Johansson, T. Bergmark, S. Karlsson, I. Lindgren, and B. Lindberg, "ESCA. Atomic Molecular and Solid State Structure Studies by Means of Electron Spectroscopy," *Nova Acta Regiae Societatis Scientiarum Upsaliensis*, vol. IV, no. 20, 1967.

[6] K. Siegbahn, C. Nordling, J. Johansson, J. Hedman, P. F. Hedén, K. Hamrin, U. Gelius, T. Bergmark, L. O. Werme, R. Manne, and Y. Baer, *ESCA applied to free molecules*. North-Holland Publishing Company, 1969.

[7] J. H. D. Eland, O. Vieuxmaire, T. Kinugawa, P. Lablanquie, R. I. Hall, and F. Penent, "Complete Two-Electron Spectra in Double Photoionization: The Rare Gases Ar, Kr, and Xe," *Physical Review Letters*, vol. 90, p. 053003, Feb 2003.

[8] J. H. D. Eland and R. Feifel, "Double ionisation of ICN and BrCN studied by a new photoelectron-photoion coincidence technique," *Chemical Physics*, vol. 327, no. 1, pp. 85–90, 2006.

[9] G. C. King and L. Avaldi, "Double-excitation and double-escape processes studied by photoelectron spectroscopy near threshold," *Journal of Physics B: Atomic, Molecular and Optical Physics*, vol. 33, no. 16, p. R215, 2000.

[10] J. Ullrich, R. Moshammer, A. Dorn, R. Dörner, L. P. H. Schmidt, and H. Schmidt-Böcking, "Recoil-ion and electron momentum spectroscopy: reaction-microscopes," *Reports on Progress in Physics*, vol. 66, no. 9, p. 1463, 2003.

[11] A. T. J. B. Eppink and D. H. Parker, "Velocity map imaging of ions and electrons using electrostatic lenses: Application in photoelectron and photofragment ion imaging of molecular oxygen," *Review of Scientific Instruments*, vol. 68, no. 9, pp. 3477–3484, 1997.

[12] H. Hertz, "Ueber einen Einfluss des ultravioletten Lichtes auf die electrische Entladung," *Annalen der Physik*, vol. 267, no. 8, pp. 983–1000, 1887.

[13] A. Einstein, “Über einen die Erzeugung und Verwandlung des Lichtes betreffenden heuristischen Gesichtspunkt,” *Annalen der Physik*, vol. 322, no. 6, pp. 132–148, 1905.
[14] A. M. Prokhorov, “Molecular amplifier and generator for submillimeter waves,” *Journal of Experimental and Theoretical Physics Letters*, vol. 7, pp. 1140–1141, Jun 1958.
[15] A. L. Schawlow and C. H. Townes, “Infrared and Optical Masers,” *Physical Review*, vol. 112, pp. 1940–1949, Dec 1958.
[16] T. H. Maiman, “Stimulated Optical Radiation in Ruby,” *Nature*, vol. 187, pp. 493–494, Aug 1960.
[17] G. S. Voronov, G. A. Delone, N. B. Delone, and O. V. Kudrevatova, “Multiphoton Ionization of the Hydrogen Molecule in the Strong Electric Field of Ruby Laser Emission,” *Journal of Experimental and Theoretical Physics Letters*, vol. 2, p. 237, 1965.
[18] L. Meitner, “Über die entstehung der β-strahl-spektren radioaktiver substanzen,” *Zeitschrift für Physik*, vol. 9, no. 1, pp. 131–144, 1922.
[19] P. Auger, “Compound Photoelectric Effect,” *Journal de Physique et Le Radium*, vol. 6, no. 6, pp. 205–208, 1925.
[20] R. Santra, “Concepts in X-ray physics,” *Journal of Physics B: Atomic, Molecular and Optical Physics*, vol. 42, no. 2, p. 023001, 2009.
[21] T. Schneider and J.-M. Rost, “Double photoionization of two-electron atoms based on the explicit separation of dominant ionization mechanisms,” *Physical Review A*, vol. 67, p. 062704, Jun 2003.
[22] T. Pattard and J. Burgdörfer, “Half-collision model for multiple ionization by photon impact,” *Physical Review A*, vol. 64, p. 042720, Sep 2001.
[23] T. Pattard, T. Schneider, and J. M. Rost, “On the role of shake-off in single-photon double ionization,” *Journal of Physics B: Atomic, Molecular and Optical Physics*, vol. 36, no. 12, p. L189, 2003.
[24] J. A. R. Samson, “Proportionality of electron-impact ionization to double photoionization,” *Physical Review Letters*, vol. 65, pp. 2861–2864, Dec 1990.
[25] S. Svensson, B. Eriksson, N. Mårtensson, G. Wendin, and U. Gelius, “Electron shake-up and correlation satellites and continuum shake-off distributions in X-ray photoelectron spectra of the rare gas atoms,” *Journal of Electron Spectroscopy and Related Phenomena*, vol. 47, pp. 327–384, 1988.
[26] M. Y. Amusia, E. G. Drukarev, V. G. Gorshkov, and M. O. Kazachkov, “Two-electron photoionization of helium,” *Journal of Physics B: Atomic and Molecular Physics*, vol. 8, no. 8, p. 1248, 1975.
[27] M. S. Schöffler, C. Stuck, M. Waitz, F. Trinter, T. Jahnke, U. Lenz, M. Jones, A. Belkacem, A. L. Landers, M. S. Pindzola, C. L. Cocke, J. Colgan, A. Kheifets, I. Bray, H. Schmidt-Böcking, R. Dörner, and T. Weber, “Ejection of Quasi-Free-Electron Pairs from the Helium-Atom Ground State by Single-Photon Absorption,” *Physical Review Letters*, vol. 111, p. 013003, Jul 2013.
[28] J. Stöhr, *NEXAFS spectroscopy*, vol. 25. Springer-Verlag Berlin, 1992.
[29] M. Cardona and L. Ley, *Photoemission in Solids I: General Principles*. Springer-Verlag, Berlin, 1978.

[30] “X-ray data booklet.” Center for X-Ray Optics and Advanced Light Source, Lawrence Berkeley National Laboratory, University of California, Berkeley, Oct 2009.
[31] J. H. D. Eland, P. Linusson, M. Mucke, and R. Feifel, “Homonuclear site-specific photochemistry by an ion-electron multi-coincidence spectroscopy technique,” *Chemical Physics Letters*, vol. 548, pp. 90–94, 2012.
[32] P. Kruit and F. H. Read, “Magnetic field paralleliser for 2π electron-spectrometer and electron-image magnifier,” *Journal of Physics E: Scientific Instruments*, vol. 16, no. 4, p. 313, 1983.
[33] P. S. Farago, *Free-electron physics*. Penguin Books, 1970.
[34] T. G. Northrop, “Adiabatic charged-particle motion,” *Reviews of Geophysics*, vol. 1, no. 3, pp. 283–304, 1963.
[35] F. Penent, J. Palaudoux, P. Lablanquie, L. Andric, R. Feifel, and J. H. D. Eland, “Multielectron Spectroscopy: The Xenon 4d Hole Double Auger Decay,” *Physical Review Letters*, vol. 95, p. 083002, Aug 2005.
[36] Y. Hikosaka, T. Aoto, P. Lablanquie, F. Penent, E. Shigemasa, and K. Ito, “Experimental investigation of core-valence double photoionization,” *Physical Review Letters*, vol. 97, p. 053003, Aug 2006.
[37] W. C. Wiley and I. H. McLaren, “Time-of-Flight Mass Spectrometer with Improved Resolution,” *Review of Scientific Instruments*, vol. 26, no. 12, pp. 1150–1157, 1955.
[38] Helmholtz-Zentrum Berlin für Materialien und Energie, “The plane grating monochromator beamline U49/2 PGM1 at BESSY II,” *Journal of large-scale research facilities*, vol. 2, no. A72, 2016.
[39] S. Plogmaker, P. Linusson, J. H. D. Eland, N. Baker, E. M. J. Johansson, H. Rensmo, R. Feifel, and H. Siegbahn, “Versatile high-repetition-rate phase-locked chopper system for fast timing experiments in the vacuum ultraviolet and x-ray spectral region,” *Review of Scientific Instruments*, vol. 83, no. 1, p. 013115, 2012.
[40] G. C. King, M. Tronc, F. H. Read, and R. C. Bradford, “An investigation of the structure near the $L_{2,3}$ edges of argon, the $M_{4,5}$ edges of krypton and the $N_{4,5}$ edges of xenon, using electron impact with high resolution,” *Journal of Physics B: Atomic and Molecular Physics*, vol. 10, no. 12, p. 2479, 1977.
[41] D. Chadwick and A. Katrib, “Photoelectron spectra of acetaldehyde and acetyl halides,” *Journal of Electron Spectroscopy and Related Phenomena*, vol. 3, no. 1, pp. 39–52, 1974.
[42] W.-C. Tam, D. Yee, and C. E. Brion, “Photoelectron spectra of some aldehydes and ketones,” *Journal of Electron Spectroscopy and Related Phenomena*, vol. 4, no. 1, pp. 77–80, 1974.
[43] K. Kimura, S. Katsumata, T. Yamazaki, and H. Wakabayashi, “UV photoelectron spectra and sum rule consideration: Out-of-plane orbitals of unsaturated compounds with planar-skeleton structure,” *Journal of Electron Spectroscopy and Related Phenomena*, vol. 6, no. 1, pp. 41–52, 1975.
[44] K. Johnson, I. Powis, and C. J. Danby, “A photoelectron-photoion coincidence study of acetaldehyde and ethylene oxide molecular ions,” *Chemical Physics*, vol. 70, no. 3, pp. 329–343, 1982.

[45] M. P. Keane, S. Lunell, A. Naves de Brito, M. Carlsson-Göthe, S. Svensson, B. Wannberg, and L. Karlsson, "Effects of relaxation and hyperconjugation on shake-up transitions in X-ray excited photoelectron spectra of some small carbonyl compounds," *Journal of Electron Spectroscopy and Related Phenomena*, vol. 56, no. 4, pp. 313–339, 1991.
[46] J. H. D. Eland, "Dynamics of Fragmentation Reactions From Peak Shapes in Multiparticle Coincidence Experiments," *Laser Chemistry*, vol. 11, no. 3-4, pp. 259–263, 1991.
[47] N. Correia, A. Naves de Brito, M. P. Keane, L. Karlsson, S. Svensson, C.-M. Liegener, A. Cesar, and H. Ågren, "Doubly charged valence states of formaldehyde, acetaldehyde, acetone, and formamide studied by means of photon excited Auger electron spectroscopy and ab initio calculations," *The Journal of Chemical Physics*, vol. 95, no. 7, pp. 5187–5197, 1991.
[48] T. X. Carroll, J. D. Bozek, E. Kukk, V. Myrseth, L. J. Sæthre, T. D. Thomas, and K. Wiesner, "Xenon $N_{4,5}OO$ Auger spectrum – a useful calibration source," *Journal of Electron Spectroscopy and Related Phenomena*, vol. 125, no. 2, pp. 127–132, 2002.
[49] D. Minelli, F. Tarantelli, A. Sgamellotti, and L. S. Cederbaum, "Advances in the theoretical simulation of Auger spectra of polyatomic molecules: an example," *Journal of Electron Spectroscopy and Related Phenomena*, vol. 74, no. 1, pp. 1–14, 1995.
[50] E. Andersson, P. Linusson, S. Fritzsche, L. Hedin, J. H. D. Eland, L. Karlsson, J.-E. Rubensson, and R. Feifel, "Formation of Kr^{3+} via core-valence doubly ionized intermediate states," *Physical Review A*, vol. 85, p. 032502, Mar 2012.
[51] Y. Hikosaka, T. Kaneyasu, E. Shigemasa, P. Lablanquie, F. Penent, and K. Ito, "Multielectron coincidence spectroscopy for core-valence doubly ionized states of CO," *The Journal of Chemical Physics*, vol. 127, no. 4, p. 044305, 2007.
[52] E. Andersson, M. Stenrup, J. H. D. Eland, L. Hedin, M. Berglund, L. Karlsson, Å. Larson, H. Ågren, J.-E. Rubensson, and R. Feifel, "Single-photon core-valence double ionization of molecular oxygen," *Physical Review A*, vol. 78, p. 023409, Aug 2008.
[53] E. Andersson, J. Niskanen, L. Hedin, J. H. D. Eland, P. Linusson, L. Karlsson, J.-E. Rubensson, V. Carravetta, H. Ågren, and R. Feifel, "Core-valence double photoionization of the CS_2 molecule," *The Journal of Chemical Physics*, vol. 133, no. 9, 2010.
[54] J. Niskanen, V. Carravetta, O. Vahtras, H. Ågren, H. Aksela, E. Andersson, L. Hedin, P. Linusson, J. H. D. Eland, L. Karlsson, J.-E. Rubensson, and R. Feifel, "Experimental and theoretical study of core-valence double photoionization of OCS," *Physical Review A*, vol. 82, p. 043436, Oct 2010.
[55] J. Niskanen, E. Andersson, J. H. D. Eland, P. Linusson, L. Hedin, L. Karlsson, R. Feifel, and O. Vahtras, "Symmetry breaking in core-valence double photoionization of SO_2," *Physical Review A*, vol. 85, p. 023408, Feb 2012.
[56] R. Murphy and W. Eberhardt, "Site specific fragmentation in molecules: Auger-electron ion coincidence studies on N_2O," *The Journal of Chemical Physics*, vol. 89, no. 7, pp. 4054–4057, 1988.
[57] C. Miron, M. Simon, N. Leclercq, D. L. Hansen, and P. Morin, "Site-Selective Photochemistry of Core Excited Molecules: Role of the Internal Energy,"

Physical Review Letters, vol. 81, pp. 4104–4107, Nov 1998.
[58] X. J. Liu, G. Prümper, E. Kukk, R. Sankari, M. Hoshino, C. Makochekanwa, M. Kitajima, H. Tanaka, H. Yoshida, Y. Tamenori, and K. Ueda, "Site-selective ion production of the core-excited CH_3F molecule probed by Auger-electron-ion coincidence measurements," *Physical Review A*, vol. 72, p. 042704, Oct 2005.
[59] P. Salén, M. Kaminska, R. J. Squibb, R. Richter, M. Alagia, S. Stranges, P. van der Meulen, J. H. D. Eland, R. Feifel, and V. Zhaunerchyk, "Selectivity in fragmentation of N-methylacetamide after resonant K-shell excitation," *Physical Chemistry Chemical Physics*, vol. 16, pp. 15231–15240, 2014.
[60] W. Eberhardt, T. K. Sham, R. Carr, S. Krummacher, M. Strongin, S. L. Weng, and D. Wesner, "Site-Specific Fragmentation of Small Molecules Following Soft-X-Ray Excitation," *Physical Review Letters*, vol. 50, pp. 1038–1041, Apr 1983.
[61] K. Müller-Dethlefs, M. Sander, L. A. Chewter, and E. W. Schlag, "Site-Specific Excitation in Molecules at Very High Energies: Changes in Ionization Patterns of CF_3CH_3," *The Journal of Physical Chemistry*, vol. 88, no. 25, pp. 6098–6100, 1984.
[62] S.-Y. Chen, C.-I. Ma, D. M. Hanson, K. Lee, and D. Y. Kim, "Selective bond rupture in nitrous oxide stimulated by core electron excitation," *Journal of Electron Spectroscopy and Related Phenomena*, vol. 93, no. 1-3, pp. 61–79, 1998.
[63] A. Naves de Brito, S. Sundin, R. R. Marinho, I. Hjelte, G. Fraguas, T. Gejo, N. Kosugi, S. Sorensen, and O. Björneholm, "Memories of excited femtoseconds: effects of core-hole localization after Auger decay in the fragmentation of ozone," *Chemical Physics Letters*, vol. 328, no. 1-2, pp. 177–187, 2000.
[64] K. Le Guen, M. Ahmad, D. Céolin, P. Lablanquie, C. Miron, F. Penent, P. Morin, and M. Simon, "Influence of formation path on the CH_2BrCl^{2+} dissociation dynamics," *The Journal of Chemical Physics*, vol. 123, no. 8, p. 084302, 2005.
[65] H. Fukuzawa, G. Prümper, X. J. Liu, E. Kukk, R. Sankari, M. Hoshino, H. Tanaka, Y. Tamenori, and K. Ueda, "Site-selective ion pair production via normal Auger decay of free CH_3F molecules studied by electron-ion-ion coincidence spectroscopy," *Chemical Physics Letters*, vol. 436, no. 1-3, pp. 51–56, 2007.
[66] H. Levola, E. Itälä, K. Schlesier, K. Kooser, S. Laine, J. Laksman, D. T. Ha, E. Rachlew, M. Tarkanovskaja, K. Tanzer, and E. Kukk, "Ionization-site effects on the photofragmentation of chloro- and bromoacetic acid molecules," *Physical Review A*, vol. 92, p. 063409, Dec 2015.
[67] H. Fukuzawa, G. Prümper, S.-i. Nagaoka, T. Ibuki, Y. Tamenori, J. Harries, X. Liu, and K. Ueda, "Site-specific fragmentation following F 1s photoionization of free CF_3SF_5 molecules studied by electron-ion coincidence spectroscopy," *Chemical Physics Letters*, vol. 431, no. 4-6, pp. 253–256, 2006.
[68] A. Mocellin, K. Wiesner, S. L. Sörensen, C. Miron, K. Le Guen, D. Céolin, M. Simon, P. Morin, A. B. Machado, O. Björneholm, and A. Naves de Brito, "Site selective dissociation upon core ionization of ozone," *Chemical Physics*

Letters, vol. 435, no. 4-6, pp. 214–218, 2007.
[69] S. Nagaoka, Y. Tamenori, M. Hino, T. Kakiuchi, J. Ohshita, K. Okada, T. Ibuki, and I. H. Suzuki, "Site-specific fragmentation caused by Si:1s core-level photoionization of $F_3SiCH_2CH_2Si(CH_3)_3$ vapor," *Chemical Physics Letters*, vol. 412, no. 4-6, pp. 459–463, 2005.
[70] S. Nagaoka, G. Prümper, H. Fukuzawa, M. Hino, M. Takemoto, Y. Tamenori, J. Harries, I. H. Suzuki, O. Takahashi, K. Okada, K. Tabayashi, X.-J. Liu, T. Lischke, and K. Ueda, "Electron-ion-ion triple-coincidence spectroscopic study of site-specific fragmentation caused by Si:2p core-level photoionization of $F_3SiCH_2CH_2Si(CH_3)_3$ vapor," *Physical Review A*, vol. 75, p. 020502, Feb 2007.
[71] S. Nagaoka, H. Fukuzawa, G. Prümper, M. Takemoto, O. Takahashi, K. Yamaguchi, T. Kakiuchi, K. Tabayashi, I. H. Suzuki, J. R. Harries, Y. Tamenori, and K. Ueda, "A Study To Control Chemical Reactions Using Si:2p Core Ionization: Site-Specific Fragmentation," *The Journal of Physical Chemistry A*, vol. 115, no. 32, pp. 8822–8831, 2011.
[72] E. Itälä, D. Ha, K. Kooser, M. Huels, E. Rachlew, E. Nõmmiste, U. Joost, and E. Kukk, "Molecular fragmentation of pyrimidine derivatives following site-selective carbon core ionization," *Journal of Electron Spectroscopy and Related Phenomena*, vol. 184, no. 3-6, pp. 119–124, 2011.
[73] E. Ruhl, S. Price, S. Leach, and J. H. D. Eland, "Charge separation mass spectrometry: Part 2. Methyl compounds," *International Journal of Mass Spectrometry and Ion Processes*, vol. 97, no. 2, pp. 175–201, 1990.
[74] R. Locht, "The dissociative ionization of carbon dioxide below 21.22 eV. A high resolution PIPECO spectroscopic investigation," *International Journal of Mass Spectrometry and Ion Processes*, vol. 148, no. 1-2, pp. L17–L23, 1995.
[75] G. Öhrwall, M. M. Sant'Anna, W. C. Stolte, I. Dominguez-Lopez, L. T. N. Dang, A. S. Schlachter, and D. W. Lindle, "Anion and cation formation following core-level photoexcitation of CO_2," *Journal of Physics B: Atomic, Molecular and Optical Physics*, vol. 35, no. 21, p. 4543, 2002.
[76] Z. D. Pešić, D. Rolles, R. C. Bilodeau, I. Dimitriu, and N. Berrah, "Three-body fragmentation of CO_2^{2+} upon K-shell photoionization," *Physical Review A*, vol. 78, p. 051401, Nov 2008.
[77] Y. Muramatsu, K. Ueda, N. Saito, H. Chiba, M. Lavollée, A. Czasch, T. Weber, O. Jagutzki, H. Schmidt-Böcking, R. Moshammer, U. Becker, K. Kubozuka, and I. Koyano, "Direct Probe of the Bent and Linear Geometries of the Core-Excited Renner-Teller Pair States by Means of the Triple-Ion-Coincidence Momentum Imaging Technique," *Physical Reviev Letters*, vol. 88, p. 133002, Mar 2002.
[78] R. K. Kushawaha, S. Sunil Kumar, I. A. Prajapati, K. P. Subramanian, and B. Bapat, "Polarization dependence in non-resonant photo-triple-ionization of CO_2," *Journal of Physics B: Atomic, Molecular and Optical Physics*, vol. 42, no. 10, p. 105201, 2009.
[79] J. H. D. Eland, L. Andric, P. Linusson, L. Hedin, S. Plogmaker, J. Palaudoux, F. Penent, P. Lablanquie, and R. Feifel, "Triple ionization of CO_2 by valence and inner shell photoionization," *The Journal of Chemical Physics*, vol. 135, no. 13, p. 134309, 2011.

[80] J. Laksman, E. P. Månsson, C. Grunewald, A. Sankari, M. Gisselbrecht, D. Céolin, and S. L. Sorensen, "Role of the Renner-Teller effect after core hole excitation in the dissociation dynamics of carbon dioxide dication," *The Journal of Chemical Physics*, vol. 136, no. 10, p. 104303, 2012.
[81] T. Luhmann, C. Gerth, M. Groen, M. Martins, B. Obst, M. Richter, and P. Zimmermann, "Final ion-charge resolving electron spectroscopy for the investigation of atomic photoionization processes: Xe in the region of the $4d \rightarrow \epsilon f$ resonance," *Physical Review A*, vol. 57, pp. 282–291, Jan 1998.
[82] Y. Hikosaka, P. Lablanquie, F. Penent, T. Kaneyasu, E. Shigemasa, J. H. D. Eland, T. Aoto, and K. Ito, "Single, double, and triple Auger decay of the Xe 4p core-hole states," *Physical Review A*, vol. 76, p. 032708, Sep 2007.
[83] Y. Hikosaka, P. Lablanquie, F. Penent, T. Kaneyasu, E. Shigemasa, J. H. D. Eland, T. Aoto, and K. Ito, "Double Photoionization into Double Core-Hole States in Xe," *Physical Review Letters*, vol. 98, p. 183002, May 2007.
[84] A. G. Kochur, A. I. Dudenko, V. L. Sukhorukov, and I. D. Petrov, "Direct Hartree-Fock calculation of multiple Xe^{i+} ion production through inner shell vacancy de-excitations," *Journal of Physics B: Atomic, Molecular and Optical Physics*, vol. 27, no. 9, p. 1709, 1994.
[85] R. Neutze, R. Wouts, D. van der Spoel, E. Weckert, and J. Hajdu, "Potential for biomolecular imaging with femtosecond X-ray pulses," *Nature*, vol. 406, no. 6797, pp. 752–757, 2000.
[86] B. Erk, D. Rolles, L. Foucar, B. Rudek, S. W. Epp, M. Cryle, C. Bostedt, S. Schorb, J. Bozek, A. Rouzee, A. Hundertmark, T. Marchenko, M. Simon, F. Filsinger, L. Christensen, S. De, S. Trippel, J. Küpper, H. Stapelfeldt, S. Wada, K. Ueda, M. Swiggers, M. Messerschmidt, C. D. Schröter, R. Moshammer, I. Schlichting, J. Ullrich, and A. Rudenko, "Ultrafast Charge Rearrangement and Nuclear Dynamics upon Inner-Shell Multiple Ionization of Small Polyatomic Molecules," *Physical Review Letters*, vol. 110, p. 053003, Jan 2013.
[87] K. Motomura, E. Kukk, H. Fukuzawa, S.-i. Wada, K. Nagaya, S. Ohmura, S. Mondal, T. Tachibana, Y. Ito, R. Koga, T. Sakai, K. Matsunami, A. Rudenko, C. Nicolas, X.-J. Liu, C. Miron, Y. Zhang, Y. Jiang, J. Chen, M. Anand, D. E. Kim, K. Tono, M. Yabashi, M. Yao, and K. Ueda, "Charge and Nuclear Dynamics Induced by Deep Inner-Shell Multiphoton Ionization of CH_3I Molecules by Intense X-ray Free-Electron Laser Pulses," *The Journal of Physical Chemistry Letters*, vol. 6, no. 15, pp. 2944–2949, 2015.

Acta Universitatis Upsaliensis

Digital Comprehensive Summaries of Uppsala Dissertations from the Faculty of Science and Technology 1410

Editor: The Dean of the Faculty of Science and Technology

A doctoral dissertation from the Faculty of Science and Technology, Uppsala University, is usually a summary of a number of papers. A few copies of the complete dissertation are kept at major Swedish research libraries, while the summary alone is distributed internationally through the series Digital Comprehensive Summaries of Uppsala Dissertations from the Faculty of Science and Technology. (Prior to January, 2005, the series was published under the title "Comprehensive Summaries of Uppsala Dissertations from the Faculty of Science and Technology".)

Distribution: publications.uu.se
urn:nbn:se:uu:diva-301128

ACTA
UNIVERSITATIS
UPSALIENSIS
UPPSALA
2016